

Improved reservoir quality assessment by evaluating illite grain coatings, quartz cementation, and compaction – Case study from the Buntsandstein, Upper Rhine Graben, Germany

Benjamin Busch^{a,*}, Johannes Böcker^b, Christoph Hilgers^a

^a Structural Geology and Tectonics, Institute of Applied Geosciences, Karlsruhe Institute of Technology, Adenauerring 20a, 76131, Karlsruhe, Germany

^b Neptune Energy Holding Germany GmbH, Ahrensburger Straße 1, 30659, Hannover, Germany

ARTICLE INFO

Keywords:

chemical compaction
pressure dissolution
diagenesis
reservoir quality
Upper Rhine Graben
Buntsandstein

ABSTRACT

Reservoir quality (RQ) in the Buntsandstein of the Upper Rhine Graben is in the center of attention as it is a possible target formation for geothermal energy production and hydrocarbon exploration surrounding existing fields. An understanding of properties affecting reservoir quality of the target lithology is still fairly poor and the success of accurately targeting high RQ intervals is limited. This is due to the fact, that the effect of compaction and the interplay between enhanced chemical compaction (i.e. pressure dissolution of quartz grains), illitic contact coatings and quartz cementation in the lithology has been underestimated. The understanding and quantification of controlling factors on reservoir qualities in fluvio-eolian sedimentary rocks, deposited in a (semi-)arid climate has been improved in recent years and this case study highlights the benefits of detailed petrographic analyses in understanding diagenetic and compactional processes in this lithology. This is especially relevant in the observation of grain coating clay minerals, whose effect depends on their specific location, i.e. either at grain contacts between quartz grains (GTG coating) or at the interface between detrital quartz grains and the intergranular volume (GTI coating).

Illitic GTI coatings affect syntaxial quartz overgrowth precipitation, as precipitation sites are locally blocked. The negative correlation between the grain coating coverage and quartz cement volumes support these findings across multiple sample sets, and they may locally preserve intergranular porosity. Illitic GTG coatings on the other hand enhance chemical compaction (i.e. pressure dissolution) and will reduce the IG. The negative correlation between these two properties again underlines the negative effect of this process on reservoir properties. Studied samples from a deep Buntsandstein well in the central URG show low reservoir quality due to either intense quartz cementation (0.7–31.7%) or a high degree of mechanical and chemical compaction (IGV: 2.3–38.0%). Higher illitic GTG and GTI coating coverages play a substantial role in controlling reservoir quality development, as demonstrated by comparing data from other fluvio-eolian lithologies (Triassic Buntsandstein and Permian Rotliegendes) to results of this study. In relation to their respective burial histories, higher illitic GTI coating coverages always correlate with smaller syntaxial quartz cement volumes. Similarly, higher illitic GTG coating coverages always correlate with lower IGV values in the three compared sample series.

As both, the precipitation of quartz cements and compaction, are a function of the burial history, i.e. effective stresses and experienced temperatures, understanding the interaction of both these processes may enable the prediction of reservoir properties in undrilled areas.

1. Introduction

The effect of mechanical and chemical compaction on reservoir quality and the intricate interaction with authigenic mineral precipitation and dissolution and their reservoir-scale effects is generally very

well described (Paxton et al., 2002). Furthermore, the processes of chemical compaction (i.e. pressure dissolution at quartz grain contacts) enhanced by the presence of illite or muscovite has been known and studied for decades (Heald, 1955; Greene et al., 2009; Kristiansen et al., 2011). In addition to vertical effective stresses and temperature,

* Corresponding author.

E-mail address: benjamin.busch@kit.edu (B. Busch).

<https://doi.org/10.1016/j.geoen.2024.213141>

Received 22 January 2024; Received in revised form 8 July 2024; Accepted 11 July 2024

Available online 14 July 2024

2949-8910/© 2024 The Authors. Published by Elsevier B.V. This is an open access article under the CC BY license (<http://creativecommons.org/licenses/by/4.0/>).

controlling compaction processes (Stephenson et al., 1992), illite and muscovite have been described to enhance the effect of chemical compaction (Bjørkum, 1996; Oelkers et al., 1996; Sheldon et al., 2003). However, modern reservoir quality studies often focus on the geochemical alteration and sometimes neglect simple and cost-effective petrography-based analyses of the degree of compaction in conjunction with petrophysical analyses to gain insight into the reservoir quality development.

In case of the Upper Rhine Graben (URG) in southwestern Germany and eastern France especially the reservoir quality of the Lower Triassic Buntsandstein sandstones receives attention, as it locally hosts oil reservoirs (Plein, 1993; Böcker, 2015), geothermal reservoirs (Dezayes et al., 1995, 2008; Griffiths et al., 2016; Heap et al., 2017), and fault and fracture hosted ore mineralizations (including galena, barite, fluorite, goethite, and others) (Held and Günther, 1993; Werner, 2012). Geothermal applications also assess the simultaneous production of lithium from formation waters hosted in sedimentary rocks (Sanjuan et al., 2016; Slunitschek et al., 2021) to increase the business case of deep geothermal production.

Hydrocarbon production success from the Buntsandstein has been restricted to the Römerberg field near Speyer (Fig. 1, Reinhold et al., 2016). Some geothermal projects in the URG are also in operation (e.g. Insheim, Landau, and Bruchsal (in Germany), Soultz-sous-Fôrets and Rittershoffen (in France), Fig. 1 a). Open-hole sections of these wells are often placed in the tight crystalline basement and the overlying clastic Permian and Triassic Buntsandstein sedimentary rocks. The interest in exploring the Buntsandstein for geothermal energy production is due to the high geothermal gradient between 50 and 72 °C/km (Haffen et al., 2015). The development of reservoir quality in the Buntsandstein, however, especially since the Eocene URG basin formation, is affected by the complex tectonic, thermal, and fluid history (Clauser and Vilinger, 1990; Böcker, 2020) and is still not fully understood.

Mechanical and chemical compaction as a function of burial depth, and fluid-rock interactions related to the experienced thermal exposure over time have been highlighted to be the main controls on reservoir properties in other siliciclastic successions. The detrital mineralogy, which is a function of the sediment source area (Allen, 2017), and the rheology of different rock fragments control the compactional behavior of siliciclastic rocks (Lander and Walderhaug, 1999; Paxton et al., 2002). Furthermore, fluid-rock interactions can e.g., reduce the intergranular porosity by quartz cement precipitation (Bjørlykke and Egeberg, 1993),

whereas samples containing well developed grain coatings contain less quartz cements and more intergranular porosity may be preserved (Bloch et al., 2002). However, the precipitation of cements may also reduce the effect of mechanical and chemical compaction and preserve the intergranular volume and porosity (Paxton et al., 2002).

Aside from inhibiting syntaxial overgrowth cementation, clay mineral grain coatings can affect permeability depending on the grain coating clay mineral textures (Heald and Larese, 1974; Busch et al., 2017). Samples characterized by pore-lining clay minerals have on average higher permeabilities than samples containing pore-bridging clay mineral textures at the same porosity (Neasham, 1977).

The grain coating clay mineral textures in the Buntsandstein from the URG has previously been reported to be mainly tangential and radial illite textures in addition to (pigmented) hematite rims (Busch et al., 2022b). These illite textures were also correlated to differences in the compactional behavior and reservoir properties, with tangential illite present at grain contacts (enhancing compaction), whereas radial illite mostly occupy grain surfaces in contact with the IGW (inhibiting syntaxial quartz precipitation, cp. Busch et al., 2018a) in samples from Permian Rotliegendes sandstones. The enhanced chemical compaction at quartz-muscovite/illite interfaces has previously been related to electrochemical surface potentials enhancing the solubility of quartz (Greene et al., 2009; Kristiansen et al., 2011) and has been described to affect porous sandstones in general (Heald, 1955).

1.1. Grain coating textures and their relation to depositional subenvironments

As grain coatings in sedimentary rocks appear in a variety of textures (e.g., Busch et al., 2020), here we only introduce the relevant textures for this study. Furthermore, we differentiate the grain coatings, depending on the interface they are covering. As proposed by Monsees et al. (2020) we differentiate into grain-to-grain (GTG, outlined in orange in Fig. 2 a) and grain-to-IGW (GTI, outlined in green in Fig. 2 a) coatings.

Pigmented hematite dust rims often occur surrounding detrital grains and at grain contacts and are readily overgrown by syntaxial mineral precipitation (grain 5 in Fig. 2 b).

Tangential illite grain coatings may completely (grain 1 in Fig. 2 b) or partially (grains 2, 4, 8 in Fig. 2 b) envelop detrital grains. They often appear as GTI coatings (grain 1 and 2 in Fig. 2 b), or as GTG coatings

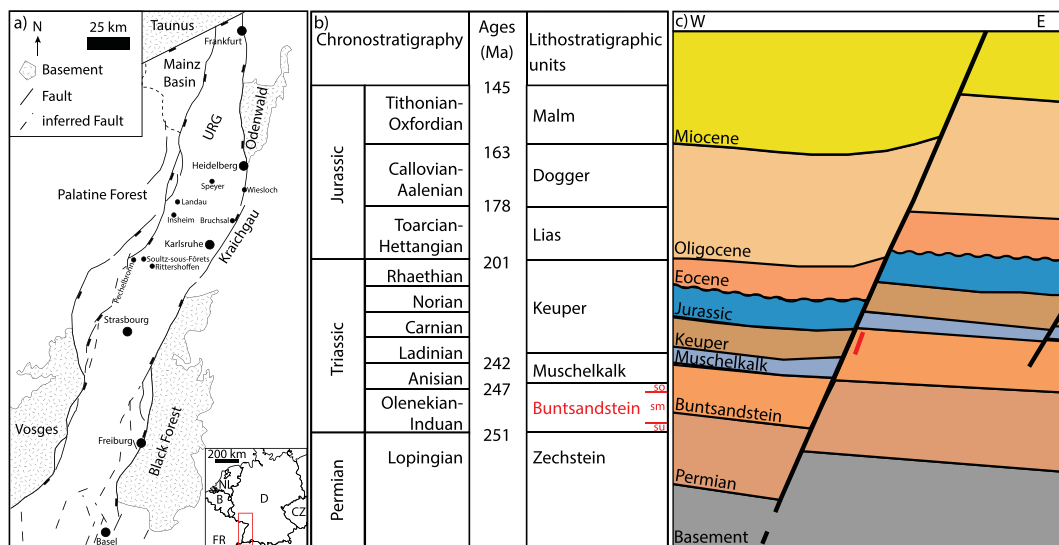


Fig. 1. a) Overview of the Upper Rhine Graben (URG). b) Chronostratigraphic and lithostratigraphic chart of the studied area (modified after Böcker and Littke (2015)). so: Upper Buntsandstein, sm: Middle Buntsandstein, su: Lower Buntsandstein. c) W-E cross-section through the studied area (section redrawn and modified after Boigk (1981)). The studied well section in the footwall of a graben-parallel fault is indicated as a red line.

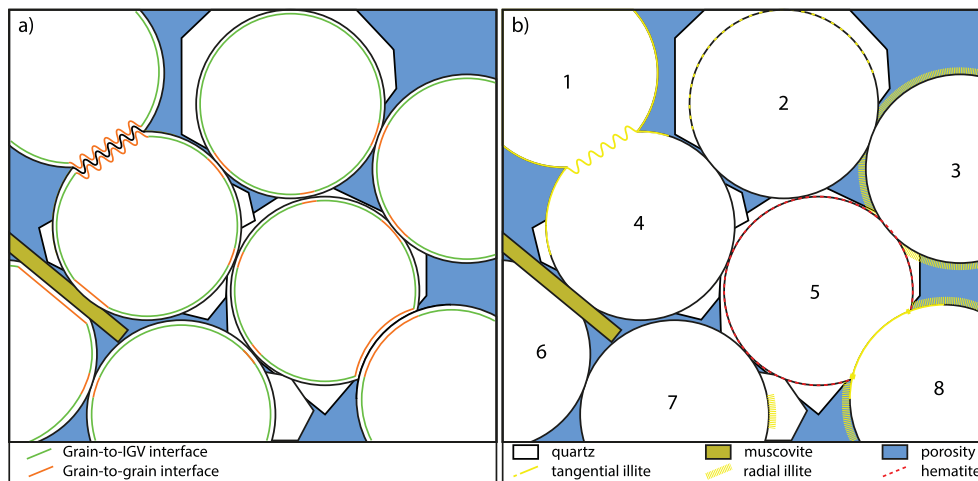


Fig. 2. a) Overview of the different interfaces to be considered for this study. b) Overview of relevant grain coating textures for the presented case study.

(grains 1 + 4 in Fig. 2 b). In areas of illitic GTG coatings sutured or concavo-convex grain contacts are often observed, indicating chemical compaction (grains 1 + 4, 5 + 8 in Fig. 2 b). For this process to be effective, it does not matter if both grains or only one grain contains a tangential illite coating. Another case of chemical compaction (i.e., pressure dissolution or grain contact dissolution) is located at interfaces of quartz and muscovite particles (grains 4 + 6 in Fig. 2 b), where quartz grains are preferentially dissolved.

Radial illitic coatings on the other hand are only occurring as GTI coatings (grains 3, 7, 8 in Fig. 2 b). They may completely (grain 3, 8 in Fig. 2 b) or partially (grain 7 in Fig. 2 b) cover these interfaces. They also may on occasion overgrow previously emplaced tangential illite grain coatings (grain 8 in Fig. 2 b).

In areas where illitic GTI coatings (regardless of their texture) completely encase the reactive surface area of detrital grains (grains 1, 3, 8 in Fig. 2 b) syntaxial cement precipitation is inhibited. Incompletely developed GTI coatings (grains 2, 4, 5, 7 in Fig. 2 b) are overgrown or completely encased in syntaxial overgrowth cements.

The distribution of clay mineral grain coatings in fluvio-eolian samples has been shown to not be related to the depositional sub-environment, grain size, sorting, or skewness (e.g., Busch, 2020; Busch et al., 2020), and previous studies in the Triassic Buntsandstein also did not show a relation to depositional sub-environment or lithofacies (Busch et al., 2022a, 2022b). In recent fluvio-eolian sediments, higher grain coating coverages were related to fluvial channels and their vicinity (Esch et al., 2008; Busch, 2020). Clay mineral grain coatings were likely emplaced on grain surfaces in fluvial channels and then redeposited in nearby depositional sub-environments (Esch et al., 2008).

1.2. Aims and objective

In a study combining outcrop and well samples Busch et al. (2022b) could show that the aspect of grain coating coverages and their influence on reservoir properties in the Buntsandstein have been largely overlooked so far. However, the present-day burial depth of samples studied in these works did not exceed 1500 m. As the degree of compaction largely relates to the burial depth (and thereby the effective vertical stress, Houseknecht, 1987; Lundegard, 1992; Paxton et al., 2002), deeper burial will likely further enhance the degree of compaction and deteriorate reservoir quality.

To further assess the reservoir quality development in more deeply buried Buntsandstein samples (2950–3100 m TVD) this study evaluates core material from an exploration well in the central URG. Results are compared to previously published grain coating coverage data and outline the possibility to use these properties to more accurately assess

reservoir quality of illite coated lithologies in deeply buried sandstone lithologies worldwide, both accounting for quartz cement inhibition and enhanced chemical compaction.

2. Geological setting

The studied well is located towards the eastern graben shoulder within the central Upper Rhine Graben in Germany, north of the city of Karlsruhe (Fig. 1 a). Formed as a part of the European Cenozoic Rift System (Ziegler, 1992), the Upper Rhine Graben extends approximately 300 km from Bale (SUI) to Frankfurt/Main (GER) with an overall NNE-SSW strike and is between 30 and 50 km wide (Fig. 1 a).

The Induan to Early Anisian Buntsandstein (Fig. 1 b (Deutsche Stratigraphische Kommission, 2016)) comprises predominantly fluvial deposits formed in a semi-arid to arid continental regime at the south-western margin of the Germanic Basin. The source area is given as the Gallic-Armorian Massif in France and the London Brabant Massif to the west in Belgium (Bourquin et al., 2006). Depositional subenvironments are mostly classified as braided rivers, fringed by alluvial, lacustrine and aeolian environments, predominantly depositing sand-sized sediments (Backhaus, 1974; Dachroth, 1985; Bourquin et al., 2011). The Triassic Buntsandstein sequence can be summarized by an overall coarsening-upward sequence, deposited in an overall base-level fall during the Lower Buntsandstein, and a subsequent overall fining upward sequence deposited in a base-level fall during the Middle and Upper Buntsandstein (Junghans, 2003; Quandt et al., 2022). The fluvial systems transport clastic sediments into the central playa lake in the northern part of the Germanic Basin (Bourquin et al., 2006). The transition to the marine conditions of the Early Anisian to Early Ladinian Muschelkalk (Fig. 1 b (Deutsche Stratigraphische Kommission, 2016)) is marked by a marine ingress into the Germanic Basin during the Upper Buntsandstein from the south (Aigner and Bachmann, 1992; Feist-Burkhardt et al., 2008), depositing transgressive limestones and dolostones. The overlying Early Ladinian to Rhaetian Keuper (Fig. 1 b (Deutsche Stratigraphische Kommission, 2016)) is characterized by alterations of transgressive and regressive deposits (Ziegler, 1990) composed of evaporitic clayey, marly, and dolomitic deposits, as well as minor fluvial and marginal marine sandstones (Düringer et al., 2019). The basin continued to subside until the Jurassic, accommodating marine limestones and shales during that time (Ziegler, 1990, 1992). Uplift and erosion during the Cretaceous and Early Eocene was heterogeneous along the strike of the present-day graben and results in a general younging of strata encountered underneath the Eocene unconformity in the subcrop from north to south (Schumacher, 2002; Böcker, 2015). The subcrop of the Eocene unconformity in the studied region consists of

Lower to Middle Jurassic deposits (LGRB, 2023). The Upper Rhine Graben rift formed from the Eocene onwards and accumulated Paleogene and Neogene marine and terrestrial sediments (Reicherter et al., 2008).

During the formation of the basin, sparse rift magmatism was occurring (Keller et al., 2002) in two phases. One phase was during the middle Eocene (Horn et al., 1972) and the second phase during the Miocene (Baranyi et al., 1976).

3. Materials and methods

34 samples from the upper and middle Buntsandstein retrieved from an exploration well in the central URG were analyzed (Well C). The samples were retrieved from a depth range of 2960–3110 m (TVD, 160–175 °C present day temperature) and are located in the footwall of a graben-parallel fault (Fig. 1 c). The present day vertical effective stress reaches up to 42 MPa. Furthermore, data of 90 samples published by Monsees et al. (2020) and Busch et al. (2022a) were used to compare the findings of this study.

Rock specimen were impregnated with blue dyed epoxy resin and prepared to be 30 µm thick for petrographic analyses. Samples are treated with a combined Alizarin red S and potassium ferricyanide solution in dilute HCl (0.3%) to aid the identification of carbonate phases. All samples were analyzed with transmitted light microscopes (Leica DM-LP fitted with a Jenoptik Progres Gryphax Subra camera) to assess the texture, grain size, detrital and authigenic constituents, and optical porosity.

The quantification of mineralogy and optical porosity was achieved by point counting with a Pelcon Automatic Point Counter mounted on a Leica DM-LP microscope (e.g., Schmidt et al., 2020b). Results are based on 300 counts per thin section. Detrital compositions are plotted after Folk (1980). Grain sizes were measured on thin sections on at least 100 grains per sample (e.g. Busch et al., 2018b). Sorting was calculated from these measurements according to Folk and Ward (1957). Point-counting and grain size measurements were performed on a grid with a step length adjusted to the maximum observed grain size to gain area-weighted results (Busch et al., 2019). Point-counting results are the basis to calculate the intergranular volume (IGV) as a measure of compaction according to Paxton et al. (2002) as the sum of intergranular porosity, intergranular cements, and depositional matrix. To derive the impact of compaction and cementation on the porosity loss, COPL (compactional porosity loss) and CEPL (cementational porosity loss) values were calculated according to Lundegard (1992):

$$COPL = P_i - \frac{((100 - P_i) \times P_{mc})}{(100 - P_{mc})} \quad (1)$$

$$CEPL = (P_i - COPL) \times \frac{C}{P_{mc}} \quad (2)$$

, with P_i : initial porosity (here 45 % for fluvial sandstones), P_{mc} : minus-cement porosity, C : pore filling cement volume. Although the depositional porosity is also a function of sorting (e.g., Beard and Weyl, 1973), the P_i value was fixed at 45 % to allow comparison of the different samples.

The assessment of grain coating coverages include both the GTG and GTI coating coverage using comparator images from Monsees et al. (2020) on at least 50 quartz grains per sample. Using the comparator images, the grain coating coverage of individual grains was categorized to fall into different classes in 10 % intervals (similar to the approach of Wooldridge et al., 2017). The comparator images and the associated grain coating coverages were determined by image analysis using ImageJ. First, the grain circumference in contact with the IGV and coated by a clay mineral phase is measured and then divided by the total grain circumference in contact with the IGV, giving the fraction of the available reactive surface area covered by a clay mineral grain coating

(GTI coating coverage). The same approach was used for the GTG coating coverage at grain contacts. The average of the 50 analyses for each type defines the reduction in surface area of detrital quartz grains in contact with the IGV per sample (GTI coating coverage) and the relative contact area between two quartz grains covered by illite or muscovite (GTG coating coverage).

As porosity and permeability data are confidential, in addition to point counted porosity (determining intergranular and intragranular porosity) thin section porosity was evaluated by image analysis in ImageJ using a consistent color threshold to segment the blue-dyed epoxy resin and the function “Analyze Particles” to gain 2D porosity values used as proxies from thin section scans.

Furthermore, a 1D burial model for the studied well was provided by the consortium partners, to assess the temperature and depth reconstructions over time. The burial model was calibrated using vitrinite reflectance data (VRo) and present-day temperatures. The eroded thickness of Jurassic and Cretaceous deposits in the region was adjusted to match VRo values below the present-day base of the Tertiary deposits. For a further discussion on burial modelling in the region, the readers are referred to Böcker (2015). 1D burial models used for comparison in the discussion chapter are derived from literature (Schwarzer and Littke, 2007; Monsees et al., 2020) or adapted to match present day depths and temperatures of the studied lithologies (Bossennec et al., 2021).

4. Results

4.1. Petrography

4.1.1. Texture

Grain sizes in the studied samples range from fine ($N = 9$) to medium sand ($N = 25$) with average grain sizes ranging from 0.133 mm to 0.379 mm. Sorting ranges from moderate to well, of which eight samples are well sorted, 22 samples are moderately well sorted, and four samples are moderately sorted.

4.1.2. Detrital composition

The most prominent detrital components are quartz grains (Fig. 3 a, b, f, h) ranging from 47.7% to 71.0%, with an average of 55.8%. K-feldspar grains (Fig. 3 a) range from 2.7% to 12.7% with an average of 6.9%, while plagioclase grains are rare (0–0.3%, avg. < 0.1%). Rock fragments (RF) are prominent in all studied samples, comprising metamorphic rock fragments (quartzites, phyllites, undifferentiated MRF, Fig. 3 b, g, h), sedimentary rock fragments (shale, siltstone, sandstone, chert, limestone, Fig. 3 b, e, f), undifferentiated plutonic rock fragments (Fig. 3 b), and undifferentiated ductile rock fragments. The undifferentiated ductile rock fragments have been heavily compacted, which obstructs clear identification of the original rock texture or structure (Fig. 3 g, h, supplementary materials 1). Metamorphic rock fragments range from 0 to 15.3% (avg. 3.6%) with the largest group being phyllites (Fig. 3 a). Sedimentary rock fragments in the studied samples range from 1 to 11.3% (avg. 4.1%), with shale RF (Fig. 3 g, h) being the most abundant, although in individual samples limestone RF are very prominent (up to 6.7%, Fig. 3 e, f). Plutonic rock fragments are present in all but seven samples and range in content from 0 to 1.7% (Fig. 3 b). The undifferentiated ductile RF content is ranging from 0 to 12.3% (avg. 1.2%) and they are present in all but eight samples.

Detrital accessory mineral grains are mostly micas (muscovite, biotite, and chlorite, Fig. 3 c, d, h), iron oxide grains, tourmaline, rutile/titanite (Fig. 3 c), as well as zircon (supplementary material). On average, they compose 0.9% of the samples (0–10.7%).

The studied samples can thus be classified as subarkoses, sublitharenites, lithic arkoses, feldspathic litharenites and litharenite (Fig. 4).

4.1.3. Authigenic composition

The main authigenic products in the studied samples are syntaxial

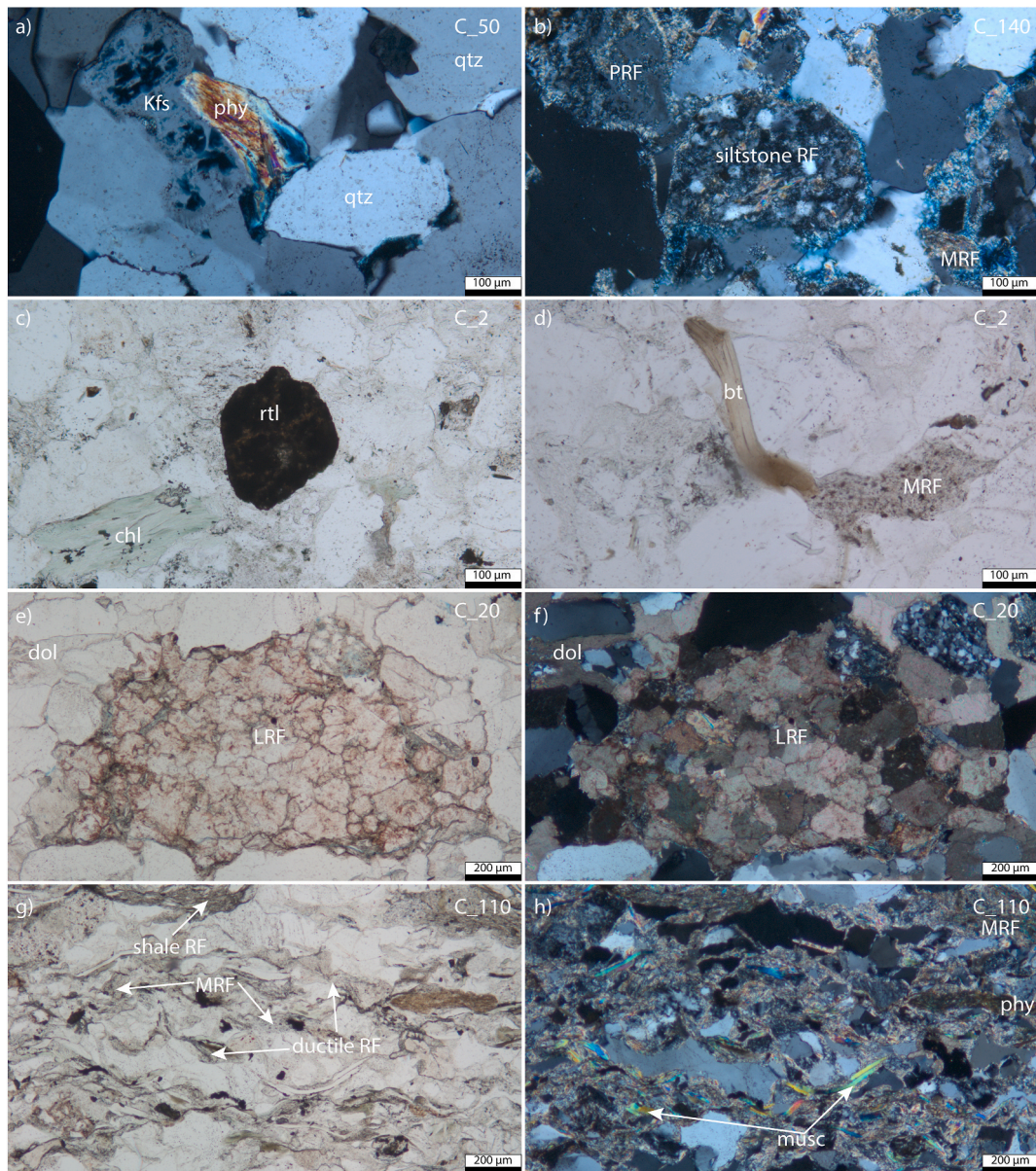


Fig. 3. a) Detrital quartz, K-feldspar, and phyllite grains. The K-feldspar grains exhibit intragranular dissolution voids. b) Metamorphic, plutonic, and siltstone rock fragment. c) Detrital rutile/titanite and chlorite grains embedded between quartz grains. d) Biotite mica and deformed metamorphic rock fragment. e, f) Calcitic detrital limestone RF (stained red) embedded between quartz grains encased in poikilotopic dolomite cement, (e: plane-polarized light (ppl), f: cross-polarized light (xpl)). g, h) Metamorphic, shale, ductile, phyllite rock fragments and muscovite flakes embedded in compacted sandstone sample. bt: biotite, cem: cement, chl: chlorite, dol: dolomite, Kfs: K-feldspar, LRF: limestone rock fragment, MRF: metamorphic rock fragment, musc: muscovite, phy: phyllite, PRF: plutonic rock fragment, qtz: quartz, RF: rock fragment, rtl: rutile.

quartz overgrowth cements, dolomite, K-feldspar overgrowth cements, siderite, radial and pore-filling illite, and iron oxide precipitates (supplementary materials 1). In individual samples chlorite ($n = 1$), solid hydrocarbon residue ($n = 1$), and barite ($n = 9$) were additionally point-counted. Replacive authigenic phases are mostly dolomite, siderite, illite and kaolinite replacing K-feldspar, as well as illite replacing kaolinite.

Syntaxial quartz overgrowth contents range from 0.7 to 31.7% (avg. 18.3%) and often exhibit euhedral crystal facets (Fig. 5 b, d - h). Quartz overgrowth cements encase pigmented hematite rims (Fig. 5 h), and only quartz grain surfaces completely covered by tangential and radial illite rims, are devoid of syntaxial cement precipitation (Fig. 5 a).

Syntaxial K-feldspar overgrowth cements are ranging from 0 to 2% (avg. 0.6%) and are encased by quartz overgrowth cements (Fig. 5 h) and on occasion also in dolomite nodules (Fig. 5 c).

Dolomite cement contents range from 0 to 25% (avg. 2.4%). Two

different dolomite cement textures are observed. A poikilotopic dolomite texture is developed mostly in nodules, where detrital quartz grains are seemingly “floating” without contacts or only exhibiting point-contacts (Fig. 5 a, b, c). Quartz grains in dolomite nodules lack any overgrowth cement, while quartz grains on the outside of the nodule are encased in quartz overgrowth cements (Fig. 5 a, b). The poikilotopic dolomite cement is also observed around detrital calcitic limestone rock fragments (Fig. 3 e, f), where quartz grains are also lacking overgrowth cements. The second dolomite texture also appears as a poikilotopic cement texture, but encases euhedral quartz overgrowth cements (Fig. 5 d) and does not preserve floating or point contacts, but is present in already compacted intergranular pores (Fig. 5 e). The dolomite also fills intragranular porosity in K-feldspar grains (Fig. 5 d).

Siderite cement was point-counted in eight samples and ranges in content from 0 to 1.3% (avg. 0.2%). The siderite is encasing dolomite in

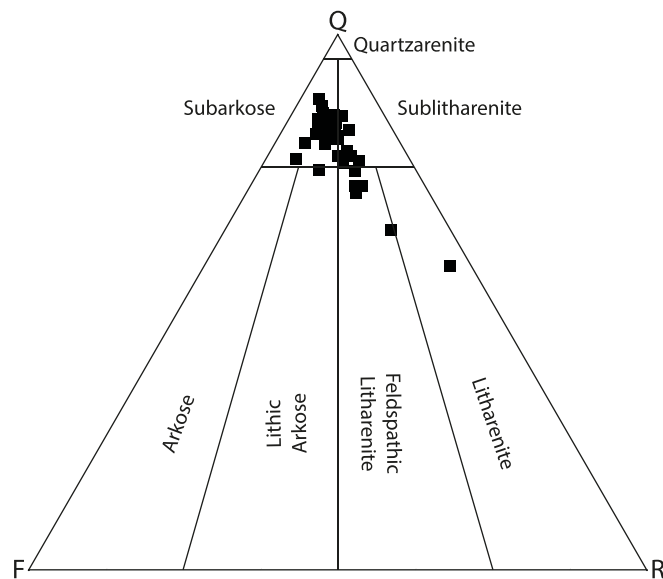


Fig. 4. Detrital composition and sandstone classification of studied Buntsandstein samples from well C.

the center and encases euhedral quartz overgrowth cements on the outside (Fig. 5 e). Furthermore, it fills some intragranular dissolution porosity in K-feldspar grains and shows a planar boundary to pore-filling barite (Fig. 6 c, d).

Illite occurs in two prominent textures, but mostly as a grain coating phase. Tangential illite is present as thin clay mineral films on the outline of detrital grains and are present at the interface to the IGV and other detrital grains (Fig. 7 f-h). The second texture is radial, platy to fibrous illite, including pore-filling illitic meshworks (Fig. 7 a-d). Tangential illite contents range from 0 to 12% (avg. 1.8%), whereas radial and meshwork illite contents range from 0 to 8% (avg. 1.5%). The radial illite texture and illitic meshworks in individual samples are stained by solid hydrocarbon residue (Fig. 6 e, f, Fig. 7 c, d), while in most samples it remains unstained (Fig. 7 a, b). Furthermore, the illitic meshworks are present in pores outlined by non-euhedral syntaxial quartz overgrowths (Fig. 6 e, f). The tangential illite texture is often stained red by hematite (Fig. 7 g, h). The radial illite texture is on occasion encased in syntaxial quartz cement overgrowths and in individual samples in contact with pore-filling chlorite (Fig. 6 a).

Hematite is also observed as two textural classes, i.e. a pigmented to continuous grain coating texture (Fig. 7 e) and a pore-filling texture. The mostly pigmented hematite dust rim contents range from 0 to 2.3% (avg. 0.3%), whereas the contents of the pore-filling texture range from 0 to 0.3% (avg. < 0.1%). Pigmented dust rims occur at grain contacts and are often encased by syntaxial quartz overgrowth cement (Fig. 7 e).

Chlorite is very rare and was only point-counted in one sample (0.7%), where it fills pores outlined with radial illite and is in contact with quartz overgrowth cements (Fig. 6 a). In the same sample it is observed to be encased in siderite (Fig. 6 b).

Pore-filling barite appears in nine samples and ranges in contents from 0 to 1% (avg. 0.1%). The barite cements encase euhedral quartz overgrowth cements (Fig. 5 f) and very rarely also fills intragranular dissolution pores within K-feldspar grains (Fig. 6 c, d).

In a single sample, remaining intergranular pore-space between syntaxial overgrowth cements is filled by solid hydrocarbon residue (0.3%) not staining an illitic substrate.

The most prominent replacive cement phase is dolomite replacing K-feldspar (avg. 0.5%). The dolomite partially fills the intragranular porosity following dissolution (Fig. 5 d), thus some intragranular dissolution porosity is preserved. The same process was observed for siderite (Fig. 6 c, d) but not encountered during point-counting.

In five samples, the replacements of K-feldspar by kaolinite (avg. < 0.1%) was point-counted. The kaolinite booklets incompletely fill intragranular pore spaces (Fig. 5 g), thus preserving some intragranular dissolution porosity. Only one occurrence of this kaolinite being replaced by illite has been point-counted (0.3%, Fig. 5 g). Replacements of K-feldspar by illite along the cleavage planes has been observed in 12 samples (avg. 0.2%).

4.1.4. Optical porosity

Optical porosity was divided into three different classes during point-counting. Intergranular porosity is the most prominent with an average of 0.5% (range: 0–2%) (Fig. 7 a). Intragranular porosity, following dissolution of K-feldspar grains or rock fragments are the second and third porosity types with an average of 0.3% each. Rock fragments experiencing dissolution are mostly chert (Fig. 5 h) and plutonic rock fragments containing feldspar minerals (Fig. 3 b).

As the intergranular porosity is also partially filled by radial and meshwork illite crystals, point-counted intergranular porosities will always be lower compared to other analyses, as illite will be point-counted but it is not pervasively filling the pores. Therefore, we also evaluated the optical porosity from image analysis to gain more accurate porosity values. The optical porosity from image analysis ranges from < 0.1 % to 4.0 %, with an average of 1.7% and includes all point counted porosity categories.

4.1.5. Grain coatings

Textures and mineralogy of grain coating phases vary throughout the studied samples. Radial illite rims are present on the outline of detrital grains in contact with the IGV (Fig. 7 a-d), whereas tangential illite rims are also found at grain contacts (Fig. 7 f-h). Furthermore, individual samples only contain pigmented to continuous hematite grain coatings (Fig. 7 e) and in some samples the tangential illite rims are additionally stained red by hematite (Fig. 7 g, h). Since tangential and radial grain coating textures occupy different grain interfaces, the specific evaluation of GTI and GTG coating coverages was performed. For the GTI coating coverage all grain coating mineral textures are evaluated, whereas tangential illite is the only grain coating texture, that is contributing to the GTG coating coverage.

Where the GTI coating coverage is complete, syntaxial quartz cement precipitation is inhibited and porosity is preserved (Fig. 7 a and b). However, if the GTI coating coverage is incomplete, syntaxial quartz overgrowth cements can form and encase the radial illite (Fig. 7 c, d) or hematite (Fig. 7 e) coatings. The GTI coating coverage in the studied samples ranges from 9.8 to 97.2%.

The GTG coating coverage in the studied samples ranges from 4.4 to 98.3% and is in most samples slightly higher than the GTI coating coverage (Fig. 8 a).

4.1.6. Compaction

The IGV of studied samples ranges from 2.3 to 38%. Comparing the COPL and CEPL highlights the compaction dominated loss of porosity in 20 of 34 samples (Fig. 8 b).

The petrographic observations highlight, that tangential illite is often present at sutured grain contacts (Fig. 7 f-h), enhancing the effect of chemical compaction (i.e. pressure dissolution). This correlation can also be supported by comparing the GTG coating coverage with the CEPL (Fig. 8 d) showing higher CEPL in samples containing higher GTG coating coverages, and vice versa. Furthermore, a reduction of the IGV due to chemical compaction is seemingly associated to shale rock fragments exhibiting columnar contacts with partially dissolved quartz grains (Fig. 9 a-d). However, the dissolution of quartz grains is only locally enhanced, where a mechanical contact between quartz grains and muscovite flakes is present (Fig. 9 b, d), while the shale RF ductilely deforms at sites of stress concentrations (i.e. quartz grain columns now encased in the shale RF). Aside from chemical compaction, mechanical compaction also acts in reducing the intergranular volume, especially

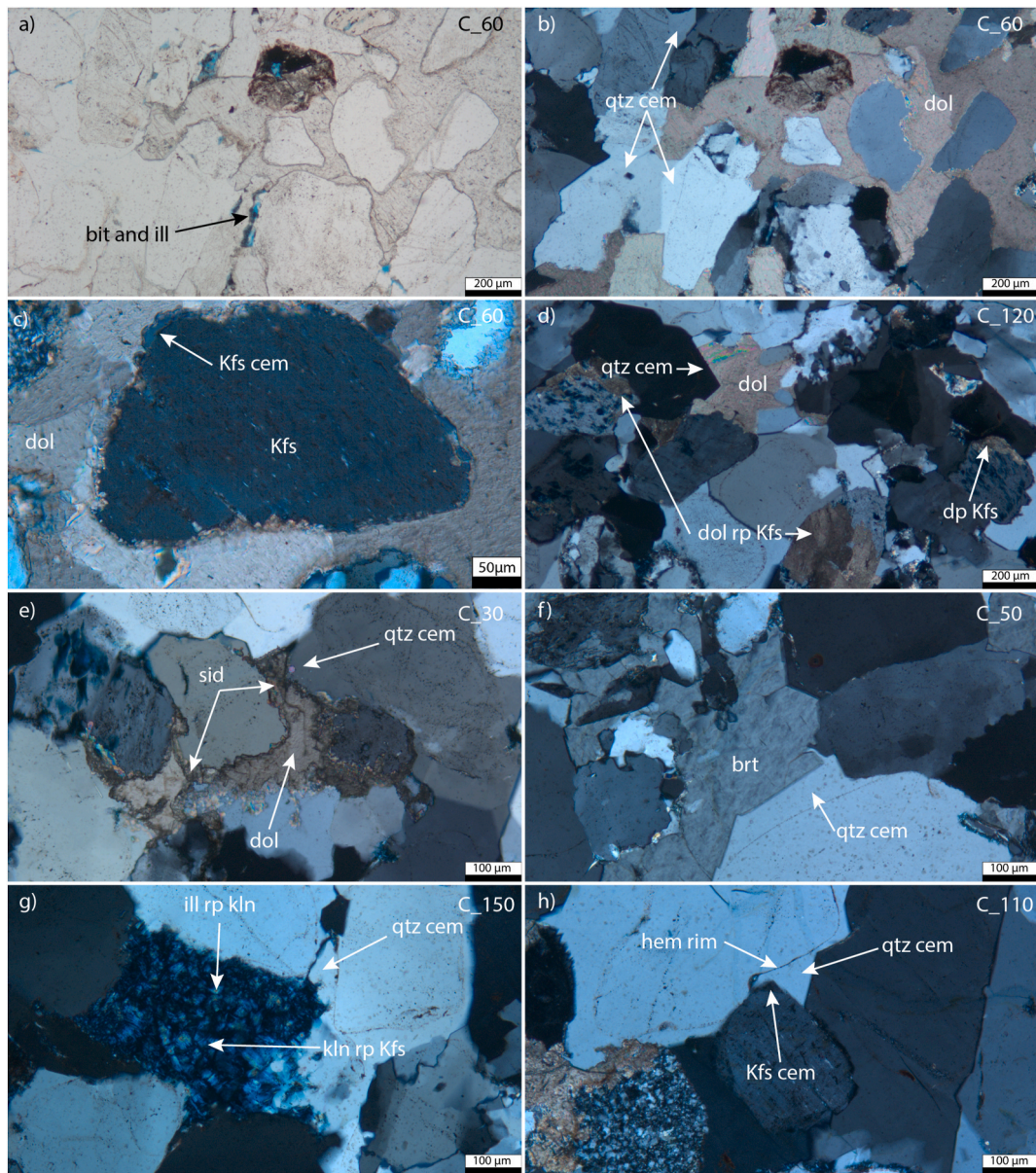


Fig. 5. a, b) Margin of dolomite nodule containing floating quartz grains. The remaining pore space is quartz cemented. Only where continuous, bitumen-stained radial illite coatings are present, overgrowth cement precipitation is inhibited (a: ppl, b: xpl). c) Syntaxial K-feldspar cement encased in dolomite nodule. d) Dolomite cement encases euhedral quartz overgrowth cement and partially replaces K-feldspar grains. Other K-feldspar grains still preserve intragranular dissolution porosity. e) Siderite encases euhedral quartz overgrowth cement. f) Barite fills remaining intergranular porosity and encases near-euhedral quartz overgrowth cements. g) Kaolinite replaces K-feldspar grain. Partially, the kaolinite is again replaced by illite. h) Syntaxial K-feldspar cement is enveloped by syntaxial quartz cement. Syntaxial quartz overgrowth cements also encase pigmented hematite dust rims. bit: bitumen, brt: barite, cem: cement, chl: chlorite, dol: dolomite, dp: dissolution porosity, hem: hematite, ill: illite, Kfs: K-feldspar, kln: kaolinite, qtz: quartz, rp: replaces, sid: siderite.

ductile rock fragments (e.g., phyllite, shale RF, and undifferentiated ductile RF) can locally affect the compaction (Fig. 9 f). However, they are not the only reason for low IGV values, as samples with low ductile RF contents below 10% show IGV values below 5% (Fig. 8 c). Furthermore, fracturing of feldspar grains along their cleavage planes can be observed (Fig. 9 e). The intragranular fractures in feldspar are also filled by quartz overgrowth cements, precipitating on neighboring grains.

4.2. Sandstone rock typing

Correlations of porosity and petrographic data allow the delineation of reservoir quality controls to derive factors and processes deteriorating or enhancing porosity and permeability to assess reservoir quality (Fig. 10, supplementary materials 1).

GTI coating coverage correlates negatively with quartz cement volumes. The smaller the available surface area for syntaxial quartz precipitation, the smaller are the volumes of syntaxial quartz overgrowth cements formed on detrital grains. This means, that larger GTI coating coverages correspond to smaller quartz cement contents (Fig. 10 a). At the same time the GTG coating coverage shows a negative correlation with the IGV indicating that larger grain contact coverage by illite affects the compactional behavior of the studied sandstone samples (Fig. 10 b). This is also indicated by the CEPL/COPL evaluations, showing samples with a high GTG coating coverage having experienced a more compaction dominated porosity loss (Fig. 8 b, c). Furthermore, the blocky cement content (non-clay mineral cements: quartz, feldspar, carbonate, and barite cements) are the main contributor to the IGV (Fig. 10 c). The IGV positively correlates with the optical porosity

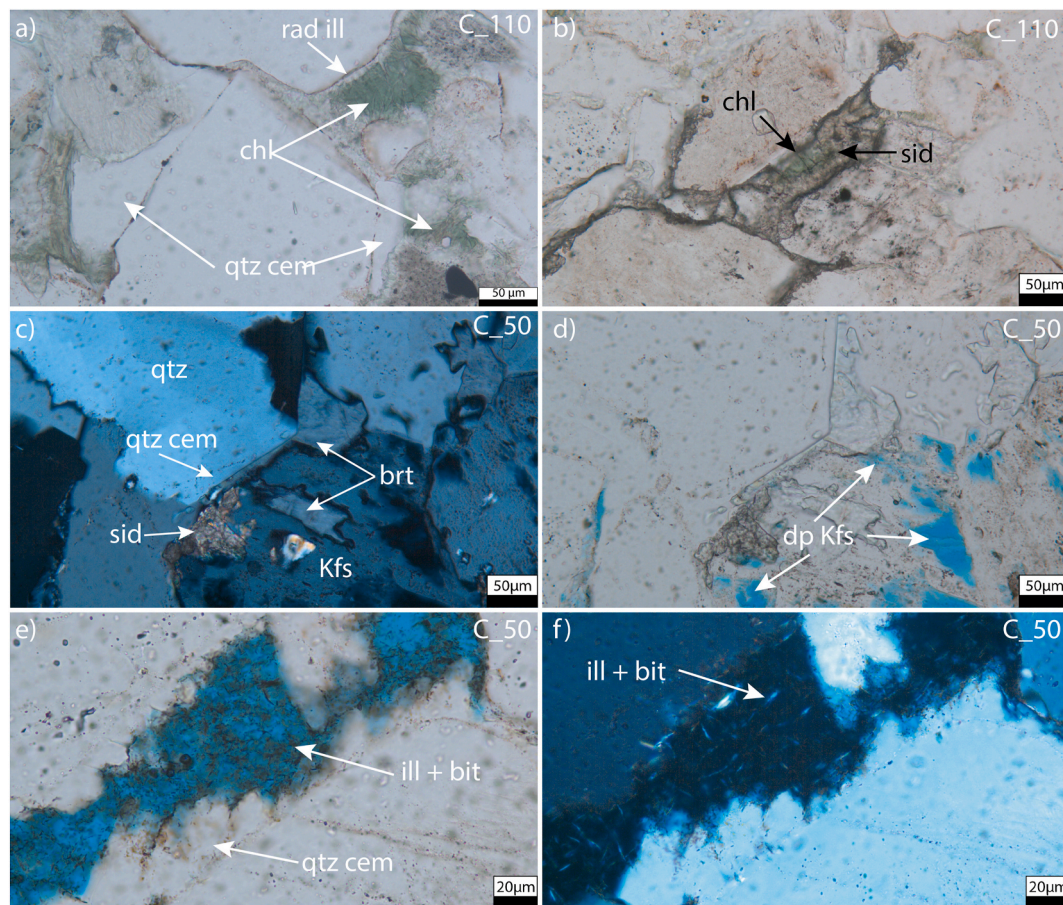


Fig. 6. a) Authigenic chlorite overgrows radial illite and quartz overgrowth cements. b) siderite encases pore-filling chlorite. c, d) Barite encasing euhedral quartz overgrowth cements and partially filling intragranular dissolution porosity in K-feldspar grain. The remaining intragranular dissolution porosity in K-feldspar grains either is filled with siderite or remains open (c: xpl, d: ppl). e, f) Hydrocarbon-stained illite meshwork filling pore-space, which is intergrown with syntaxial quartz overgrowth cements at the outline of the pores (e: xpl, f: ppl). bit: bitumen, brt: barite, cem: cement, chl: chlorite, dp: dissolution porosity, ill: illite, Kfs: K-feldspar, qtz: quartz, rad: radial, sid: siderite.

derived from image analysis (Fig. 10 d), as does the related cementational porosity loss (CEPL, Fig. 10 f). Furthermore, it can be observed that the intergranular porosity from point-counting is generally higher in samples characterized by a high IGV (Fig. 10 d). Conversely, the compactional porosity loss (COPL) negatively correlates with the optical porosity from image analysis (Fig. 10 e). If this plot is color-coded with the GTG grain coating coverage it becomes apparent, that samples with higher GTG grain coating coverage also exhibit higher COPL values and lower porosities.

Furthermore, evaluating the cement phase's individual influence on the optical porosity from image analysis, a positive correlation is observed for quartz overgrowth cements (Fig. 10 g), whereas no correlation was observed for carbonate cements (Fig. 10 h). Color-coding the quartz cement plot with the GTI grain coating coverage, it becomes apparent, that samples with higher porosity, on average have lower grain coating coverages, and therefore higher quartz cement contents, highlighting the indirect effect of grain coating illite on reservoir properties.

When assessing the effect of detrital grain size on the optical porosity derived from image analysis, a slight positive correlation might be observed, although the coefficient of determination is low ($R^2 = 0.15$). However, in combination with the color-coding for COPL values, the individual outlier at large grain sizes can be explained by higher compactional porosity loss.

5. Discussion

5.1. Paragenetic sequence

Based on the petrographic observations a paragenetic sequence is established (Fig. 11). While the paragenetic sequence is generally comparable to other previously published examples from the studied lithology within the URG, some local differences can be observed.

5.1.1. Early diagenesis

As pigmented hematite rims are encased in all other authigenic phases (Fig. 5 d, f, h, 6 e, 7 a), they are interpreted to be the earliest diagenetic phase. This is in agreement with other studies on continental red beds deposited in a semi-arid fluvio-eolian depositional system (van Houten, 1973; Walker, 1979).

Since the tangential illite coatings are locally stained red by hematite, and present at grain contacts (Fig. 7 f-h) they are interpreted to be emplaced contemporaneously with hematite precipitation, likely by illuviation. As they are present at grain contacts, they are interpreted to be emplaced prior to mechanical compaction. Furthermore, the grains containing continuous tangential illite coatings are not substrates to syntaxial quartz cement precipitation, thus their emplacement has to predate quartz cementation. The early diagenetic infiltration of tangential clay minerals is common in both, fluvio-eolian samples in general (Esch et al., 2008) and the Buntsandstein in particular (Molenaar et al., 2021). Similar observed clay mineral textures have also been related to soil formation processes in samples from Permian

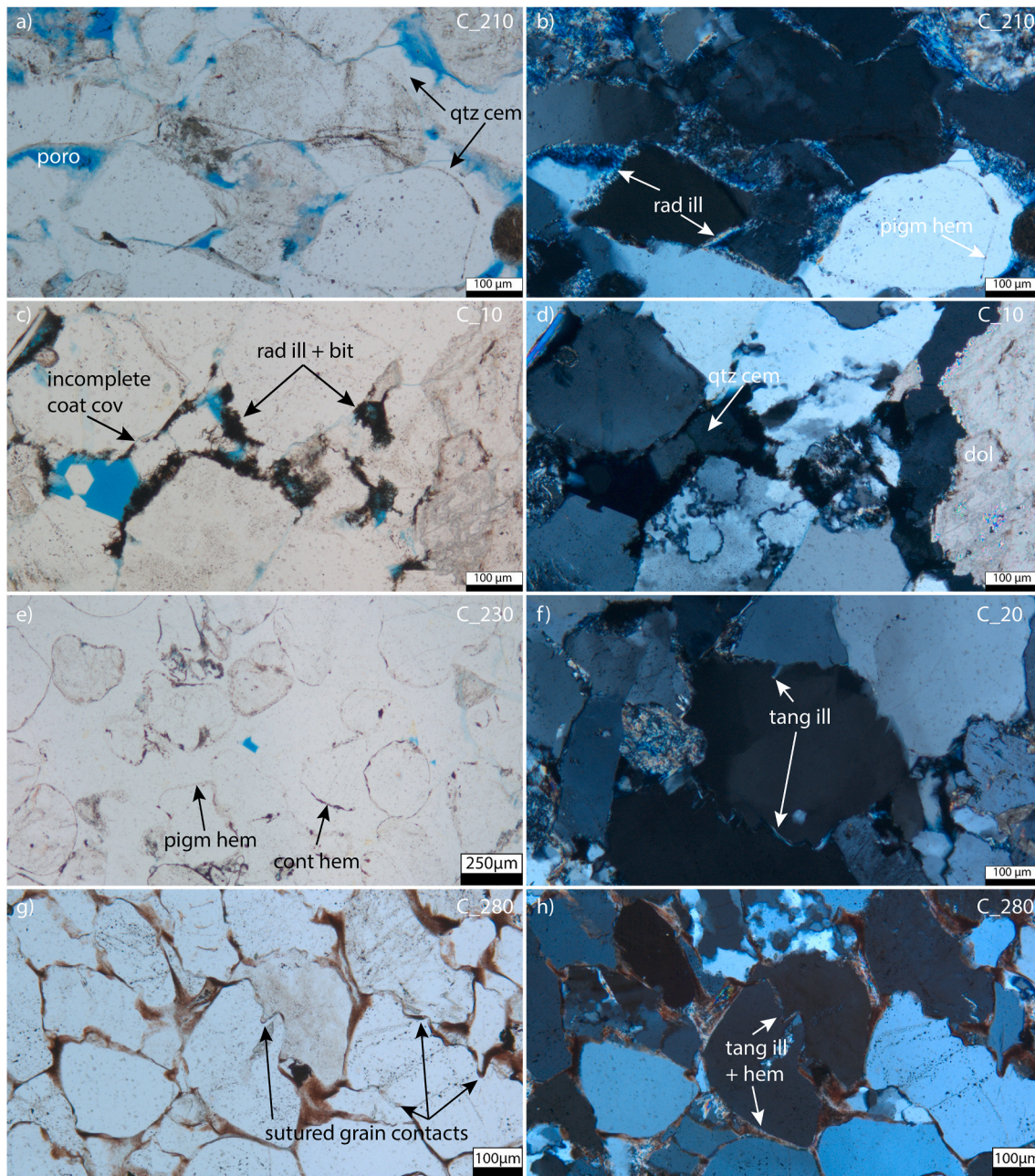


Fig. 7. a, b) Radial illite occupies the grain to IGV interfaces and inhibits syntaxial overgrowth cements, preserving porosity, whereas pigmented hematite rims are readily overgrown (a: ppl, b: xpl). c, d) Incomplete grain coating coverage by radial illite (here stained black by bitumen) results in quartz outgrowths (c: ppl, d: xpl). e) Pigmented and continuous hematite rims encasing detrital grains are encased in syntaxial quartz overgrowth cements (31.7% in this sample). f) Tangential illite rims are often present at sutured grain contacts. g, h) Even hematite-stained, reddish-brown tangential illite grain coatings are present at sutured grain contacts (g: ppl, h: xpl).

Rotliegendes red bed sandstones (Molenaar and Felder, 2018). Tangential illite grain coatings from the Rotliegendes in northern Germany indicate a recrystallization from a precursory grain coating phase during burial diagenesis (Liewig and Clauer, 2000), which might be necessary for the paragenetic sequence presented here as well. However, studies in active fluvio-eolian depositional systems in the USA also show tangential illite coatings at the time of deposition (Esch et al., 2008; Busch, 2020), so based on the sediment source area this phase of recrystallization to illite might not be necessary. The optical assessment of illite as the main grain coating mineral phase (tangential and radial) is supported by SEM-BSE and XRD analyses in other Buntsandstein samples from the region (Clauer et al., 2008; Soyk, 2015).

As the nodular, poikilotopic dolomite cement preserves a floating

grain texture, where detrital grains do not contain syntaxial overgrowth cements (Fig. 5 a, b), they are interpreted to also form prior to the initial phase of mechanical compaction. However, as dolomite cement towards the margins of the nodules (Fig. 5 a, b) also encases syntaxial quartz overgrowth cements (Fig. 5 d), a later burial diagenetic phase post- or syndating quartz precipitation is interpreted as well. Similar nodular, pre-compaction dolomite cement in semi-arid fluvio-eolian samples from Triassic red beds in the North Sea Central Graben (Lippmann, 2012) and Germany (Aehnelt et al., 2021), and have been related to pedogenic processes leading to the formation of a vadose dolocrete. In the studied samples nodule formation may also have been favored by dolomite precipitation on detrital limestone rock fragments (Fig. 3 e, f).

As syntaxial K-feldspar cements are encased by syntaxial quartz

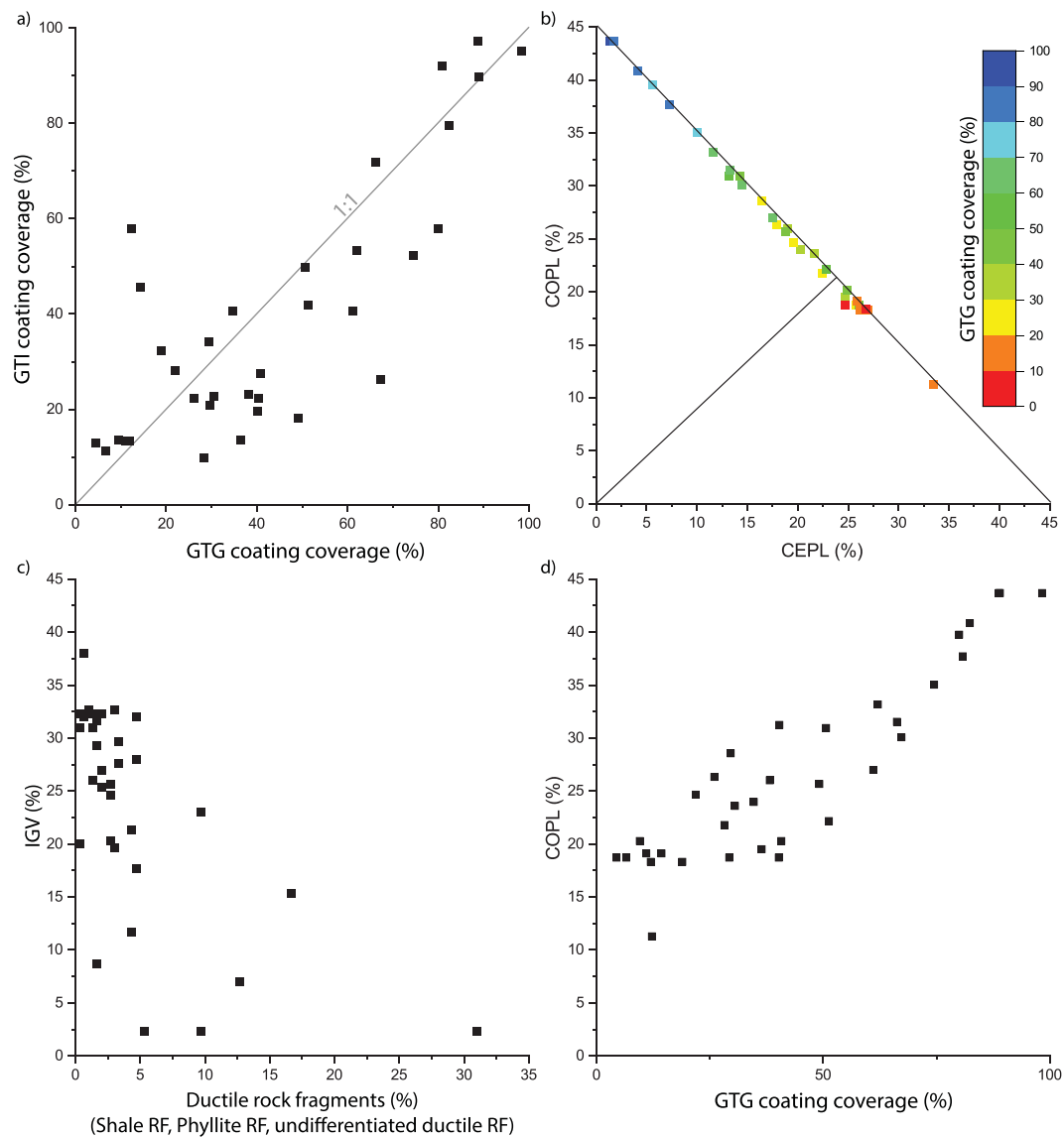


Fig. 8. a) The GTG and GTI coating coverages for each sample do not correlate with each other. b) CEPL/COPL plot color-coded for the GTG grain coating coverage. Most samples experience a compaction-dominated porosity loss and larger GTG coating coverages correspond to larger porosity loss by compaction. c) Cross plot of the amount of ductile rock fragments (shale RF, phyllite RF, and undifferentiated ductile RF) versus the IGV. Higher amounts of ductile RF do not necessarily correspond to lower IGV (and thus a higher degree of compaction). d) Cross plot of the GTG coating coverage versus the COPL. Higher GTG coating coverages correlate with higher compactional porosity loss.

cements (Fig. 5 h), and fractures in K-feldspar grains with a syntaxial overgrowth, are filled by quartz overgrowth cements precipitating on a neighboring quartz grain (Fig. 9 e), they pre- or syndate the precipitation of quartz cement and predate grain fracturing during compaction. Some K-feldspar grains encased in early diagenetic dolomite nodules also show syntaxial feldspar overgrowth cements (Fig. 5 c), indicating an early diagenetic feldspar cement phase prior to dolomite nodule formation. This early diagenetic K-feldspar cement is typical for (semi-)arid depositional environments (e.g., Füchtbauer, 1974; Schöner and Gaupp, 2005; Gaupp and Okkerman, 2011) and has also been described for similar samples from the Buntsandstein of the studied region (Busch et al., 2022a).

Mechanical compaction initiated during early diagenesis as a function of sedimentation and burial.

5.1.2. Burial diagenesis

As radial illite was observed on the outline of detrital grains in contact with the IGV (Fig. 7 a, b), and is occasionally encased by

syntaxial quartz cement (Fig. 7 c, d) it is interpreted to be one of the initial authigenic phases during burial diagenesis, prior to quartz cement precipitation. The absence of radial illite at grain contacts additionally supports a burial diagenetic origin, following the initial phase of mechanical compaction. Where the radial illite coating is continuous, quartz cement precipitation is additionally inhibited. This is in agreement with K/Ar-age dating studies on illite from the Upper Rhine Graben, showing an onset of illite precipitation in the Buntsandstein from 210 Ma extending until 95 Ma, which was previously related to hydrothermal events (Clauer et al., 2008).

The subsequent syntaxial quartz cement precipitation forms mostly euhedral syntaxial overgrowths (Fig. 5 b, d, f). They are only inhibited in areas of continuous tangential or radial illite coatings (Fig. 7). As quartz overgrowth cements are postdating dolomite nodule formation, K-feldspar cement, and radial illite, a burial diagenetic origin is interpreted, to account for the elevated temperature and previous radial illite precipitation. As the quartz precipitation rates are depending on the silica saturation, temperatures, crystallographic orientations, and

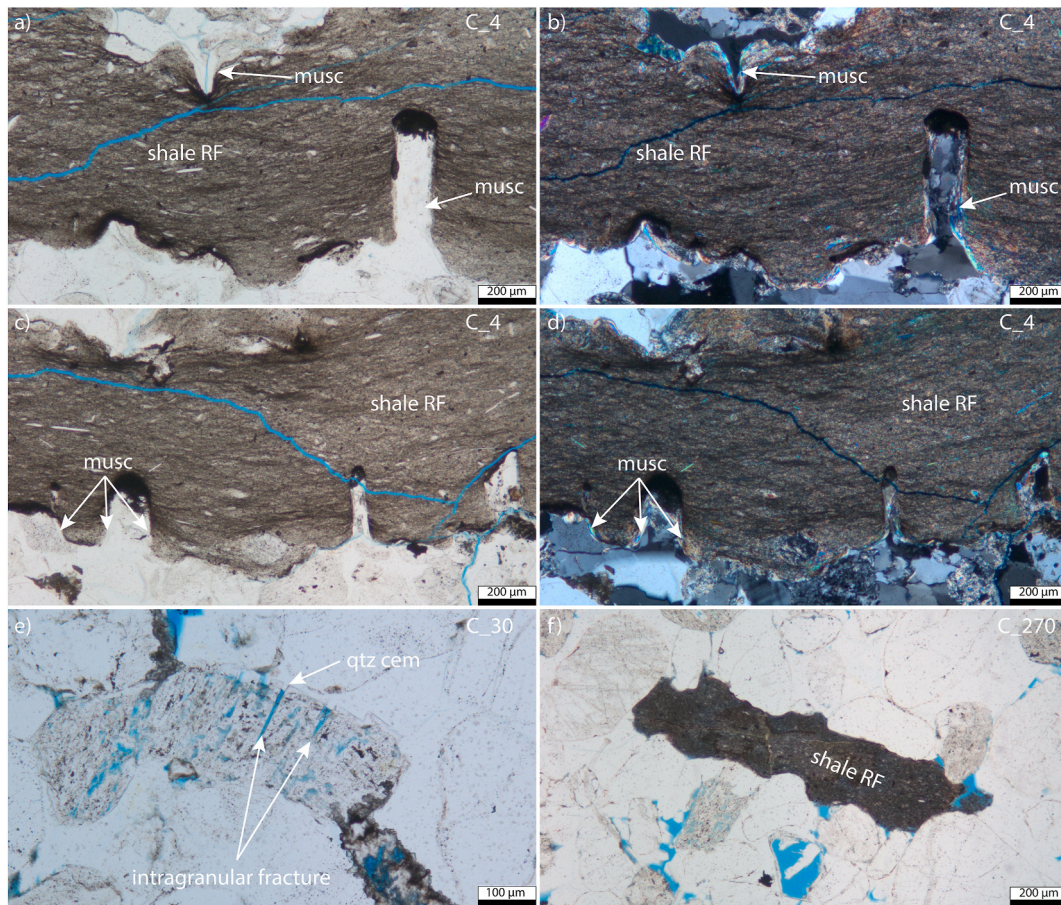


Fig. 9. a, b, c, d) Quartz columns encased in shale RF. The shale RF shows signs of ductile deformation, i.e. it gets darker in areas where it is compressed, whereas the surrounding detrital grains show sutured grain boundaries, i.e. signs of chemical compaction. The chemical compaction is especially pronounced in areas, where muscovite is present (yellow-red-blue interference colors) (a, c: ppl, b, d: xpl). e) K-feldspar grain containing a syntaxial overgrowth cement and intragranular fractures, which are filled by quartz overgrowth cement. f) Ductilely deformed shale RF between more rigid detrital quartz grains.

polycrystallinity of the substrate, rock compositions and grain coating coverage (Heald and Larese, 1974; Walderhaug, 1994b, 1994a; Lander et al., 2008; Prajapati et al., 2018, 2020; Busch et al., 2021) a burial diagenetic origin is favored. Possible sources for the silica in solution are chemical compaction at grain contacts covered with illite or in contact with micas (Kristiansen et al., 2011; Monsees et al., 2020), dissolution of K-feldspar, or clay mineral recrystallization (Worden and Morad, 2000).

As dissolution pores and replacive kaolinite within K-feldspar grains are not pervasively filled or encased by quartz cement (Fig. 5 d, e, g) but fractures crosscutting the K-feldspar grains and syntaxial overgrowth cements are partially filled by quartz cements, feldspar dissolution and kaolinite replacements are interpreted to syn- to post-date quartz cement precipitation. Due to intragranular pore space within K-feldspar grains being preserved, and not being filled by other authigenic minerals or being compacted, a burial diagenetic dissolution phase is interpreted, while the remaining grain framework has already been stabilized, mainly by quartz and carbonate cements. The remaining intragranular pore space in K-feldspar grains is not filled by quartz cement as all observed quartz cements form as syntaxial overgrowths (Fig. 5 a, b, d-h).

However, as intragranular K-feldspar porosity is filled partially with dolomite, the onset of dissolution has to predate the second phase of dolomite precipitation. This second phase of dolomite precipitation also encases euhedral quartz cements (Fig. 5 b-d) further highlighting the formation during burial diagenesis. The second phase of dolomite is also occasionally encased in siderite and shows a similar paragenesis towards a more iron-rich carbonate composition during burial diagenesis as described for other core samples from the Buntsandstein in the Upper

Rhine Graben (Busch et al., 2022a).

Kaolinite replacing K-feldspar is also on occasion recrystallized to illite (Fig. 5 g). This recrystallization is interpreted to occur during the burial diagenetic K-feldspar dissolution, as a source for K^+ -ions is required (Lanson et al., 2002). However, the illitization of kaolinite is only very rarely observed. Furthermore, as meshwork-illite in intergranular pores, which is stained by hydrocarbons, are intergrown with syntaxial quartz overgrowth cements (Fig. 6 e, f) a formation at the same time as quartz cement precipitation is interpreted. A likely source for the meshwork-illite precipitation is the dissolution of K-feldspar grains (Lanson et al., 2002). The in-situ replacement of K-feldspar is also interpreted to occur during the same time as meshwork illite precipitation.

Since chlorite, observed only in individual samples, encases both radial illite and quartz overgrowth cements (Fig. 6 a), it is interpreted to postdate radial illite precipitation and the onset of quartz cement precipitation. Additionally, chlorite being encased in siderite indicates a formation prior to siderite precipitation during burial diagenesis. As the chlorite cement fills intragranular pore spaces, and does not replace other mineral phases, it is interpreted to precipitate from solution. However, as the samples do not contain large amounts of volcanic rock fragments and chlorite predates siderite precipitation (e.g., Curtis et al., 1985), the formation is yet to be studied in further detail. It is however, likely that the Fe required for the precipitation could be derived from hematite rims, as bleaching and iron mobilization is well documented in the Buntsandstein (e.g., Bauer, 1994; Wendler et al., 2011; Schmidt et al., 2020a; Aehnelt et al., 2021).

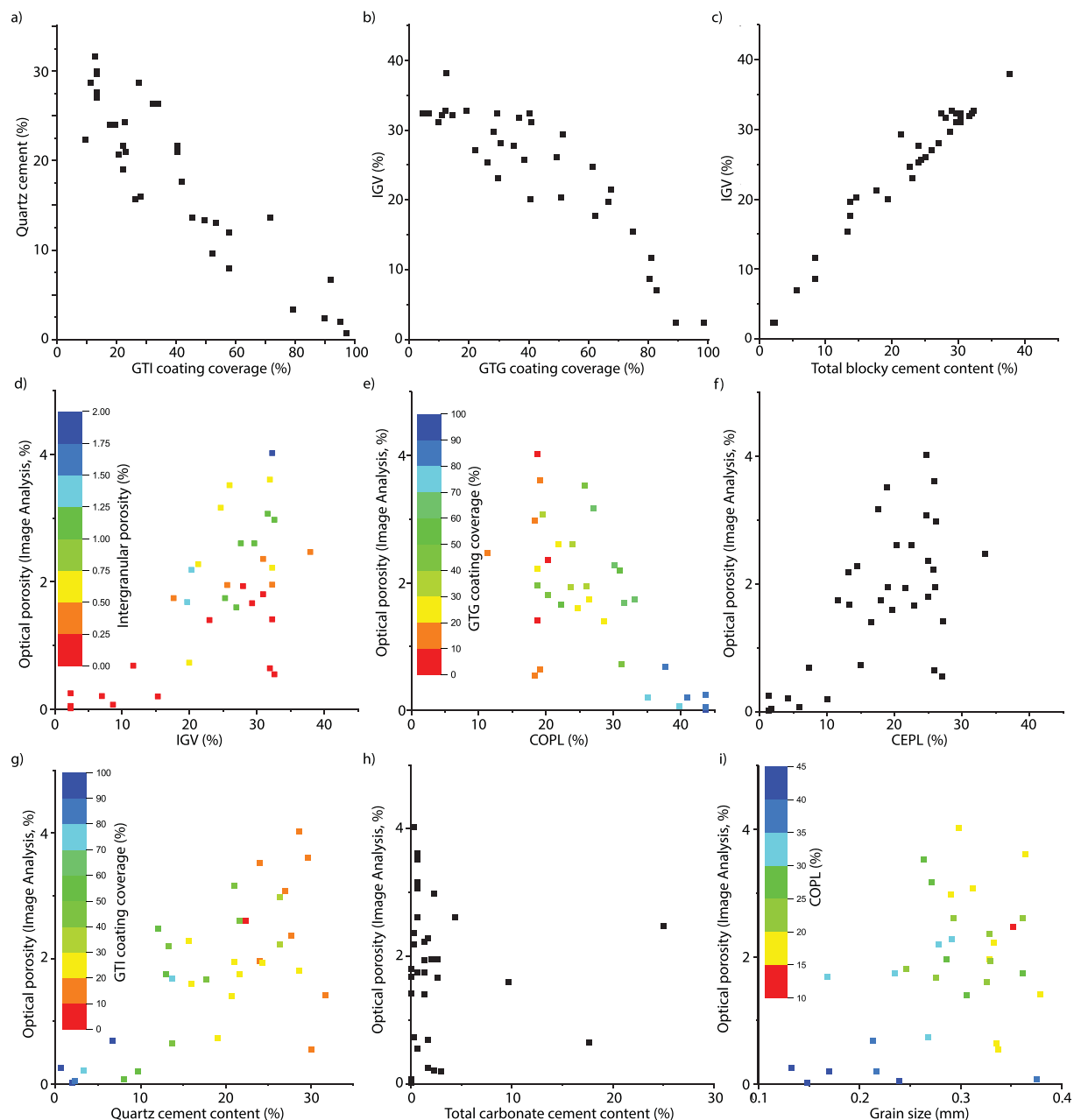


Fig. 10. a) GTI coating coverage vs. quartz cement content. b) GTG coating coverage vs. IGTV. c) IGTV vs. total blocky cement content. Optical porosity vs. d) IGTV (color-coded for intergranular porosity), e) COPL (color-coded for GTG grain coating coverage), f) CEPL, g) quartz cement content (color-coded for GTI coating coverage), h) total carbonate cement content, and i) grain size (color-coded for COPL).

The siderite cement phase is also observed to partially fill intra-granular dissolution pores in K-feldspar grains (Fig. 6 c) and encase previously precipitated dolomite (Fig. 5 e). As the pore-filling and replacive barite also encases siderite replacements in feldspar grains (Fig. 6 c, d) siderite precipitation is interpreted to pre-date the formation of barite. The required Fe for siderite precipitation also likely originated from the dissolution of hematite rims.

As barite encases euhedral quartz cement overgrowths, and only partially fills intragranular dissolution pores in K-feldspar grains, it is interpreted to postdate the start of quartz cement precipitation and interpreted to cease during burial diagenetic K-feldspar dissolution. As there is no direct paragenetic relation between barite and illite meshworks, but they both appear in the same samples (Fig. 6 c-f), their relation to quartz overgrowth cements is used as an aid in relative dating. As illitic meshworks are present in pores containing non-

euhedral syntaxial quartz overgrowths (Fig. 6 e, f) and barite encases euhedral syntaxial quartz overgrowths (Fig. 6 c, d), the formation of illitic meshworks is interpreted to predate barite precipitation. As the barite precipitation, especially in fractures in the studied region is often also associated with sulfide precipitation (e.g., Held and Günther, 1993; Werner and Dennert, 2004; Griffiths et al., 2016; Busch et al., 2022a), and fluid inclusions in fracture-filling barite from Soutz-sous-Fôrets record temperature ranges from 125 to 126 °C (Dubois et al., 1996), a hydrothermal origin is interpreted. Especially, due to the presence of sulfide ore minerals in conjunction with barite in other samples from the region, a similar age range as the Zn–Pb–Ag MVT deposit (dated to the Miocene (Pfaff et al., 2010)) is interpreted for the barite precipitation in the studied samples.

One of the last diagenetic modifications is the emplacement of hydrocarbons, now staining radial and meshwork illite, thus postdating

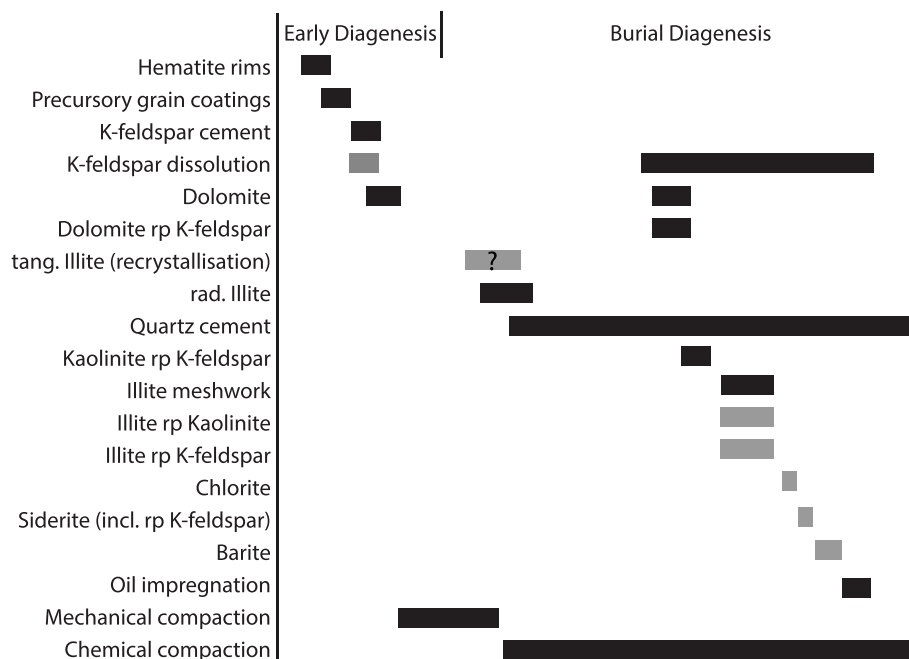


Fig. 11. Simplified paragenetic sequence based on the paragenetic observations in thin sections. Grey boxes indicate diagenetic phases only observed in individual samples, the question mark indicates an uncertain phase. rad: radial, rp: replaces, tang: tangential.

both phases. As hydrocarbon-stained radial illite is encased in syntaxial quartz overgrowth cements (Fig. 7 c), the hydrocarbon emplacement is interpreted to occur during the late stages of quartz precipitation. Including the reconstructed hydrocarbon expulsion phase from Liassic source rocks in the region from the Oligocene to Miocene (Böcker and Littke, 2015), a late burial diagenetic origin is interpreted. The encasement of hydrocarbon stained radial illite in quartz overgrowth cements also indicates that quartz cement precipitation occurred continuously following the precipitation of radial illite and continued after hydrocarbon emplacement. However, as only illite appears to be oil-wet, a relation to other authigenic phases cannot be reconstructed.

Chemical compaction initiated along grain contacts covered by tangential illite and at quartz muscovite interfaces during burial diagenesis and contributed to the precipitation of quartz cement overgrowths during burial diagenesis and likely continues until present day.

5.2. Reservoir quality controls

Optical porosity determination by image analysis often underestimates the porosity values from petrophysical measurements, as microporosity in e.g., clay minerals cannot be resolved optically. However, the relative match between optical porosity from image analysis and petrophysical measurements was checked and maintained throughout the presented samples series. Thus, optical porosities approximate petrophysical porosities, but petrophysical values will be higher. Therefore, general controlling parameters on porosity can still be delineated.

Based on the rock typing plots (Fig. 10) and COPL/CEPL evaluations (Fig. 8 b) the main controls on reservoir quality in the studied samples are compactional porosity loss and burial diagenetic quartz cement precipitation. Both of these processes are related and may affect one another: Quartz cement content initially stabilizes the grain framework against further compaction, whereas intense mechanical and chemical compaction reduces the IGV (and thereby porosity) in which quartz cement could precipitate.

However, the quartz cement contents are much higher than in sandstones of a similar detrital composition but shallower maximum burial depth, resulting in lower optical porosities <5% (Fig. 10 g) when

compared to the results of Busch et al. (2022a). While the positive correlation between optical porosity from image analysis and quartz cement content is still visible, this is in stark contrast to samples from a shallower depth, where the syntaxial quartz cement counteracted the compaction and preserved porosity (Busch et al., 2022a). While the tangential and radial illite grain coatings also affect the formation of syntaxial quartz cement, locally inhibiting them (Fig. 6 a-d, Fig. 10 a, g), the high thermal exposure results in further quartz cement precipitation, which ultimately encases the radial illite grain coatings (Fig. 7 c).

The degree of compaction in the studied samples appears to be largely influenced by the presence of tangential illite grain coatings and their effect on chemical compaction (Fig. 10 b, e). While they may locally inhibit syntaxial quartz cement precipitation, the tangential grain coatings affect the compactional behavior much more, thus resulting in a porosity loss, rather than porosity preservation by inhibition of quartz cement precipitation. The dominance of compactional processes on reservoir properties is also supported by the positive correlation of IGV and CEPL with optical porosities from image analysis. Highest porosities are observed in samples containing higher cementational porosity loss and which are less compacted and therefore have higher IGV. The indirect effect of tangential grain coating phases on porosity via chemical compaction is supported by the evaluations of optical porosities and COPL color-coded for the GTG coating coverage (Fig. 10 e), showing a negative correlation, i.e. highest COPL/lowest porosities in samples with a higher GTG coating coverage. The effect of carbonate cements on porosities in the studied samples is indeterminate (Fig. 10 h). Only individual samples containing a high carbonate cement content show above average optical porosities from image analysis. This can be related to the early diagenetic carbonate cement nodules stabilizing the grain framework against further compaction (Busch et al., 2022b). The correlation of grain size and optical porosities from image analysis is generally still positive (Fig. 10 i), which is in agreement with previous studies in the Buntsandstein (Kunkel et al., 2018; Busch et al., 2022b; Quandt et al., 2022), but it is overprinted by the COPL reducing the coefficient of correlation. As the COPL is not related to grain size, but rather the presence of GTG coating coverage and the content of ductile rock fragments (Fig. 8 c).

Directly relating the porosity values to permeabilities is not straight-

forward, as samples containing radial illite grain coatings and illitic meshworks will likely have lower permeabilities than samples containing tangential grain coatings at the same porosities (see also Neasham, 1977).

5.3. Comparison to previously published results and implications for reservoir quality prediction modeling

Grain coating coverages and their effect on quartz cementation are fairly well studied (e.g., Heald and Larese, 1974; Pittman et al., 1992; Bloch et al., 2002), and the presence of illite at sutured grain contacts and their effect on chemical compaction have been described before (Heald, 1955). The understanding of driving forces of chemical compaction processes has also been improved in recent years e.g., by the works of Greene et al. (2009) and Kristiansen et al. (2011) highlighting

the effect of electrochemical surface potentials in enhancing pressure dissolution of quartz at quartz-illite/muscovite interfaces. Their experiments show a dissolution rate proportional to voltage, electron charge, and temperature (eq. (2) in Greene et al., 2009) and they state that pressure (i.e. effective vertical stress) plays an important role in maintaining the contact between two dissimilar materials (Kristiansen et al., 2011). However, a quantification of the contact coverage and the relation to compactional behavior was not attempted prior to the works of Monsees et al. (2020), (2021), although the effect of illitic grain coating texture on compaction was noticed by Busch et al. (2018a). The simple and yet effective assessments of grain coating coverages are thus an essential part in evaluating controlling factors on reservoir quality development. In this section we will be comparing the GTG and GTI coating coverages from two available studies performed on fluvio-eolian subsurface core samples, both deposited in a (semi-)arid climate

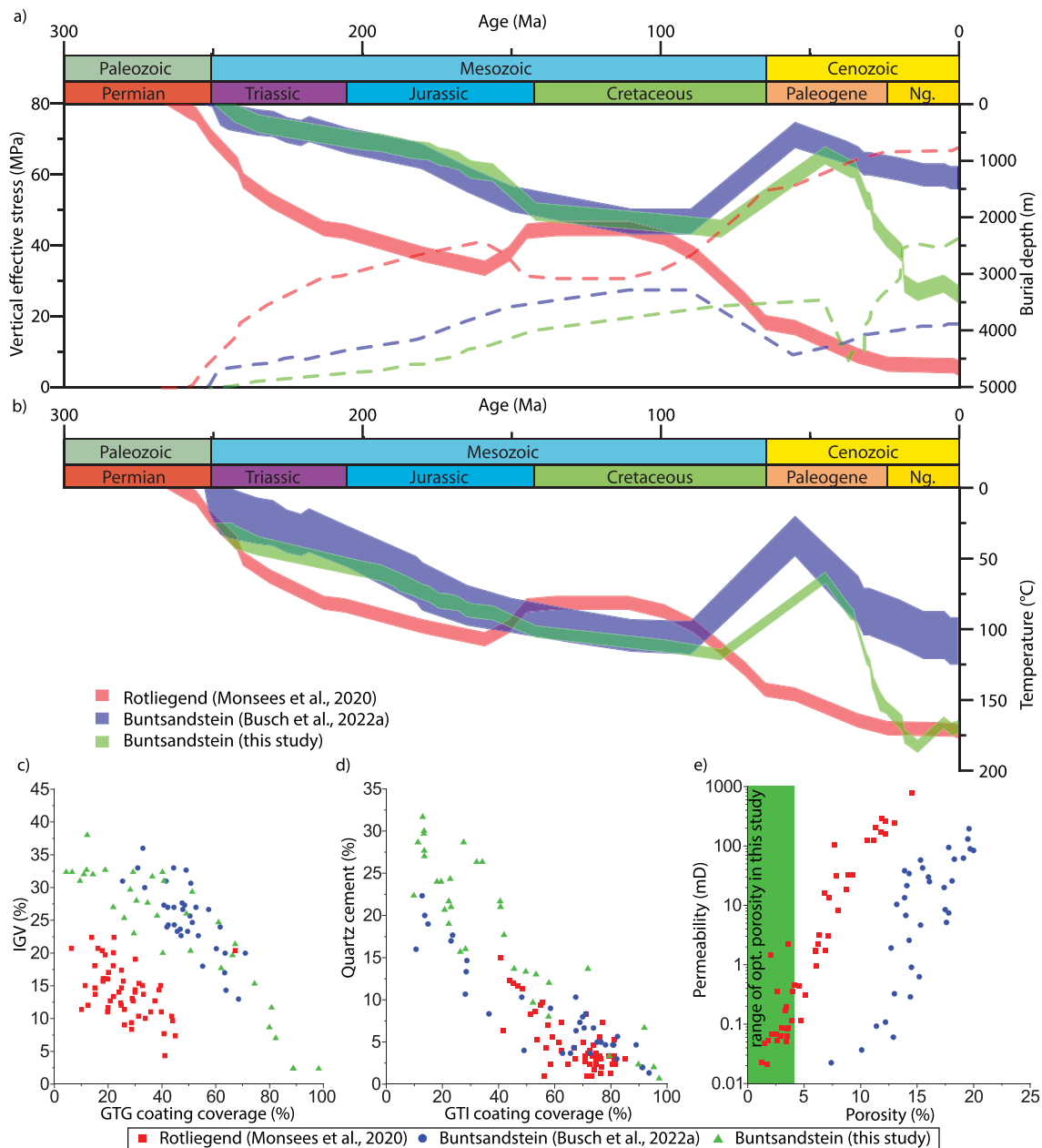


Fig. 12. a) Burial depth (filled areas) and effective vertical stress (dashed lines) reconstruction for the studied reservoir lithologies. The depth range covers thickness of the studied formation, vertical effective stresses are given for the base of the formation. b) Temperature reconstruction for the studied reservoir lithologies. c) Cross-plot of GTG coating coverage against the IGV. d) Cross-plot of the GTI coating coverage against the quartz overgrowth cement content. e) Porosity-permeability cross plot. Ng: Neogene.

containing illitic grain coatings (Rotliegend samples from northern Germany in Monsees et al., 2020; Buntsandstein samples from the URG in Busch et al., 2022a) and the samples of this study in relation to their burial histories as they are the only available subsurface datasets to consistently compare the findings of this study (Fig. 12).

When assessing the effect of GTG coating coverages with the burial depth reconstructions (Fig. 12 a), the effect of greater maximum burial depths, vertical effective stresses, and higher thermal exposure of the Rotliegendes sample series (red dataset) becomes apparent. The Rotliegendes samples of Monsees et al. (2020) exhibit a similar range of IGW values as the Buntsandstein samples from Busch et al. (2022a), however lower GTG coating coverages are recorded in the Rotliegendes samples (Fig. 12 c). Although the GTG coating coverage is lower in the Rotliegendes sample series, the vertical effective stresses (Fig. 12 a) and thermal exposure (Fig. 12 b) affecting the samples is higher, and therefore the IGW is further reduced as a function of burial depth, mostly since the Cretaceous. The range of recorded IGW values for the presented Buntsandstein series of this work (green dataset) is much larger and also covers a wider range of GTG coating coverages. However, when assessing the ranges in which IGW and GTG coating coverages overlap, smaller GTG coating coverages are required to achieve the same IGW values, which is in agreement with the overall deeper burial in this part of the URG than in the study area from Busch et al. (2022a) (blue dataset).

The effect of the GTI coating coverage in relation to the thermal exposure (i.e. experienced temperature during the burial history), which affects the precipitation kinetics of quartz, is less apparent at first glance. This is likely related to the overall high degree of coverage for the Rotliegendes dataset (Fig. 12 d). However, when comparing the two Buntsandstein datasets, the dataset which experienced a lower thermal exposure (blue dataset) contains smaller quartz cement contents than the samples from this study, which experienced a higher thermal exposure. This effect is visible especially at GTI coating coverages <70%. As the samples from the present study experienced higher temperatures during burial, more quartz cement could precipitate. This is due to the kinetics of quartz cement precipitation, where elevated temperatures increase the reaction kinetics (e.g., Rimstidt and Barnes, 1980; Lander et al., 2008). As the Rotliegendes samples show a smaller spread of GTI coating coverages at values above 40% the resulting quartz cement volumes are all below 15%, although the thermal exposure is much higher than experienced by either Buntsandstein dataset (Fig. 12 b, d).

The resulting porosities and permeabilities (Fig. 12 e) of the studied sample series are a function of their diagenetic histories including their compaction. The sample series showing the lowest thermal exposure and shallowest burial (blue dataset) contains the highest porosity, related both to high IGW and small syntaxial cement volumes (especially in poorly grain coated samples (<40% GTI coating coverage) (Fig. 12 e). The Rotliegendes sample series (red dataset) experienced the highest thermal exposure, but has the highest average GTI coating coverage, therefore comparably small quartz cement volumes. However, due to the prolonged deep burial since the Cretaceous, the effect of compaction, slightly enhanced by illitic GTG coatings, resulted in IGW values mostly below 25% and therefore reduced the porosity, while permeability is still fairly high (Fig. 12 e). The present Buntsandstein dataset (green dataset) shows comparable GTI and GTG grain coating ranges as the other Buntsandstein dataset, but due to higher thermal exposure, especially since the Eocene graben formation, quartz cement volumes are higher. Furthermore, the deeper burial resulted in a more intense compaction, enhanced by the illitic GTG coatings, resulting in much lower porosities (Fig. 12 e).

Understanding and correctly assessing these processes can enable the prediction of reservoir properties. The effect of GTI coating coverage on syntaxial quartz precipitation are already well understood and included in simulation tools such as Touchstone™ (Makowitz et al., 2006; Lander et al., 2008; Tamburelli et al., 2022) or Exemplar™ (Walderhaug, 1996;

Lander et al., 1997; Lander and Walderhaug, 1999; Walderhaug et al., 2000). These simulation approaches also include the assessment of mechanical compaction based on grain rigidities and the effect of compaction on reservoir properties (Lander and Walderhaug, 1999). Including the effect of GTG coating coverages may be an efficient additional constraint to simulate the effect of chemical compaction extending the known controls of vertical effective stress and temperature (Stephenson et al., 1992; Sheldon et al., 2003). This may also bridge the gap in better assessing the internal sources of quartz in solution, as chemical compaction, (i.e. pressure dissolution or stylolization) is often given as a main supply of dissolved silica in formation fluids (e.g., Heald, 1955; Sibley and Blatt, 1976). This approach will also require a better understanding of the distribution of grain coating mineral phases in sedimentary deposits, as they may be variably preserved or abraded in remobilized fluvio-eolian deposits (Ajdukiewicz et al., 2010) and a clear correlation to depositional sub-environments or grain size is rarely observed (Busch, 2020).

6. Conclusions

The compaction-dominated porosity loss in the studied samples is strongly affected by grain-to-grain coating coverages, which deteriorate reservoir quality. The degree of compaction cannot just be correlated to the mineralogical composition of detrital rock fragments, and therefore the assessment of GTG coating coverages in illite-coated sandstones may be an essential tool in assessing reservoir quality controls and predicting RQ in undrilled areas. While the grain-to-IGW coating coverages have a measureable influence on the content of quartz cements, the integration with burial histories of studied samples is still essential, as the thermal exposure additionally affects the rate at which quartz cements can precipitate.

Furthermore, the presented results highlight that the grain coating coverage in contact with the IGW or at grain contacts should be evaluated individually, as they are not directly comparable. Tangential illitic grain coatings are present at grain contacts and in contact with the IGW, thus affect both, the enhanced chemical compaction and syntaxial quartz precipitation, whereas radial illitic grain coatings are absent at grain contacts, and only affect syntaxial quartz precipitation. The necessity to assess the grain coating coverage in two separate classes may facilitate future pre-drill predictions of the reservoir quality and enhance the success of subsurface operations in hydrocarbon, geothermal, or underground gas storage projects.

CRedit authorship contribution statement

Benjamin Busch: Writing – original draft, Visualization, Methodology, Investigation, Formal analysis, Conceptualization. **Johannes Böcker:** Writing – review & editing, Resources, Methodology. **Christoph Hilgers:** Writing – review & editing, Visualization, Investigation, Conceptualization.

Declaration of competing interest

The authors declare that they have no known competing financial interests or personal relationships that could have appeared to influence the work reported in this paper.

Data availability

All research data is included in a supplementary data file.

Acknowledgements

BB and CH thankfully acknowledge sample and data provision by Neptune Energy Holding Deutschland GmbH, Rhein Petroleum GmbH, and Palatina GeoCon GmbH & Co. KG. The authors thankfully

acknowledge constructive review comments by the anonymous reviewers.

Appendix A. Supplementary data

Supplementary data to this article can be found online at <https://doi.org/10.1016/j.geoen.2024.213141>.

References

- Aehnelt, M., Hilde, U., Pudlo, D., Heide, K., Gaupp, R., 2021. On the origin of bleaching phenomena in red bed sediments of Triassic Buntsandstein deposits in Central Germany. *Geochemistry* 125736. <https://doi.org/10.1016/j.chemer.2020.125736>.
- Aigner, T., Bachmann, G.H., 1992. Sequence-stratigraphic framework of the German Triassic. *Sediment. Geol.* 80, 115–135.
- Ajdukiewicz, J.M., Nicholson, P.H., Esch, W.L., 2010. Prediction of deep reservoir quality using early diagenetic process models in the Jurassic Norphlet Formation, Gulf of Mexico. *AAPG (Am. Assoc. Pet. Geol.) Bull.* 94 (8), 1189–1227. <https://doi.org/10.1306/04211009152>.
- Allen, P.A., 2017. *Sediment Routing Systems - the Fate of Sediment from Source to Sink*. Cambridge University Press, Cambridge CB2 8BS, United Kingdom.
- Backhaus, E., 1974. *Limnische und fluviatile Sedimentation im südwestdeutschen Buntsandstein*. *Geol. Rundsch.* 63 (3), 925–942.
- Baranyi, L., Lippolt, H.J., Todt, W., 1976. Kalium-Argon-Altersbestimmungen an tertiären Vulkaniten des Oberrheingraben-Gebietes: II. Die Alterstraverse vom Hegau nach Lothringen. *Oberrheinische geologische Abhandlungen* 24, 41–62.
- Bauer, A., 1994. Diagenese des Buntsandsteins im Bereich der Rheingraben-Weststrandstörung bei Bad Dürkheim. *Mitt. Pollichia* 81, 215–289.
- Beard, D.C., Weyl, P.K., 1973. Influence of texture on porosity and permeability of unconsolidated sand. *AAPG (Am. Assoc. Pet. Geol.) Bull.* 57 (2), 349–369.
- Bjørkum, P.A., 1996. How important is pressure in causing dissolution of quartz in sandstones? *J. Sediment. Res.* 66 (1), 147–154.
- Bjørlykke, K., Egeberg, P.K., 1993. Quartz cementation in sedimentary basins. *AAPG (Am. Assoc. Pet. Geol.) Bull.* 77 (9), 538–548.
- Bloch, S., Lander, R.H., Bonnell, L.M., 2002. Anomalously high porosity and permeability in deeply buried sandstone reservoirs: origin and predictability. *AAPG (Am. Assoc. Pet. Geol.) Bull.* 86, 301–328. <https://doi.org/10.1306/61EEDABC-173E-11D7-8645000102C1865D>.
- Böcker, J., 2015. *Petroleum System and Thermal History of the Upper Rhine Graben*. RWTH Aachen University, p. 168. PhD thesis.
- Böcker, J., 2020. Hydrothermal influences in the Römerberg oil field and their impacts on reservoir diagenesis. *DGMK/ÖGEG Frühjahrstagung 2020*. Celle, Germany.
- Böcker, J., Littke, R., 2015. Thermal maturity and petroleum kitchen areas of liassic black shales (lower jurassic) in the central upper rhine graben, Germany. *Int. J. Earth Sci.* 105 (2), 611–636. <https://doi.org/10.1007/s00531-015-1188-9>.
- Boigk, H., 1981. *Erdöl und Erdgas in der Bundesrepublik Deutschland*. Erdölprovinzen, Felder, Förderung, Vorräte. Lagerstättentechnik. Enke, Stuttgart, Germany, p. 330.
- Bossennec, C., Gérard, Y., Böcker, J., Klug, B., Mattioni, L., Sizun, J.-P., Sudo, M., Moretti, I., 2021. Evolution of diagenetic conditions and burial history in Buntsandstein Gp. fractured sandstones (Upper Rhine Graben) from in-situ $\delta^{18}O$ of quartz and $40Ar/39Ar$ geochronology of K-feldspar overgrowths. *Int. J. Earth Sci.* <https://doi.org/10.1007/s00531-021-02080-2>.
- Bourquin, S., Bercovici, A., López-Gómez, J., Diez, J.B., Broutin, J., Ronchi, A., Durand, M., Arché, A., Linol, B., Amour, F., 2011. The Permian–Triassic transition and the onset of Mesozoic sedimentation at the northwestern peri-Tethyan domain scale: palaeogeographic maps and geodynamic implications. *Palaeogeogr. Palaeoclimatol. Palaeoecol.* 299 (1–2), 265–280. <https://doi.org/10.1016/j.palaeo.2010.11.007>.
- Bourquin, S., Péron, S., Durand, M., 2006. Lower Triassic sequence stratigraphy of the western part of the Germanic Basin (west of Black Forest): fluvial system evolution through time and space. *Sediment. Geol.* 186 (3–4), 187–211. <https://doi.org/10.1016/j.sedgeo.2005.11.018>.
- Busch, B., 2020. Pilot study on provenance and depositional controls on clay mineral coatings in active fluvio-eolian systems, western USA. *Sediment. Geol.* 406, 105721 <https://doi.org/10.1016/j.sedgeo.2020.105721>.
- Busch, B., Adelmann, D., Herrmann, R., Hilgers, C., 2022a. Controls on compactional behavior and reservoir quality in a Triassic Buntsandstein reservoir, Upper Rhine Graben, SW Germany. *Mar. Petrol. Geol.* 136, 105437 <https://doi.org/10.1016/j.marpetgeo.2021.105437>.
- Busch, B., Adelmann, D., Hilgers, C., 2018a. Reservoir quality modeling in deeply-buried Permian Rotliegendes sandstones. In: *N-Germany. Impact of illite textures, EAGE Conference and Exhibition*, pp. 1–5. EAGE, Copenhagen.
- Busch, B., Becker, I., Koehrer, B., Adelmann, D., Hilgers, C., 2019. Porosity evolution of two Upper Carboniferous tight-gas-fluvial sandstone reservoirs: impact of fractures and total cement volumes on reservoir quality. *Mar. Petrol. Geol.* 100, 376–390. <https://doi.org/10.1016/j.marpetgeo.2018.10.051>.
- Busch, B., Hilgers, C., Adelmann, D., 2020. Reservoir quality controls on Rotliegend fluvio-aolian wells in Germany and The Netherlands, Southern Permian Basin – impact of grain coatings and cements. *Mar. Petrol. Geol.* 112, 104075 <https://doi.org/10.1016/j.marpetgeo.2019.104075>.
- Busch, B., Hilgers, C., Gronen, L., Adelmann, D., 2017. Cementation and structural diagenesis of fluvio-aolian Rotliegend sandstones, northern England. *J. Geol. Soc.* 174, 855–868. <https://doi.org/10.1144/jgs2016-122>.
- Busch, B., Hilgers, C., Lander, R.H., Bonnell, L.M., Adelmann, D., 2018b. Reservoir quality and burial model evaluation by kinetic quartz and illite cementation modeling: case study Rotliegendes, N-Germany. *AAPG (Am. Assoc. Pet. Geol.) Bull.* 101 (2), 293–307. <https://doi.org/10.1306/0503171605217075>.
- Busch, B., Okamoto, A., Garbev, K., Hilgers, C., 2021. Experimental fracture sealing in reservoir sandstones and its relation to rock texture. *J. Struct. Geol.* 153, 104447 <https://doi.org/10.1016/j.jsg.2021.104447>.
- Busch, B., Spitzner, A.-D., Adelmann, D., Hilgers, C., 2022b. The significance of outcrop analog data for reservoir quality assessment: a comparative case study of Lower Triassic Buntsandstein sandstones in the Upper Rhine Graben. *Mar. Petrol. Geol.* 141 <https://doi.org/10.1016/j.marpetgeo.2022.105701>.
- Clauer, N., Liewig, N., Ledesert, B., Zwingmann, H., 2008. Thermal history of Triassic sandstones from the Vosges Mountains-Rhine Graben rifting area, NE France, based on K-Ar illite dating. *Clay Miner.* 43 (3), 363–379. <https://doi.org/10.1180/claymin.2008.043.3.03>.
- Clouser, C., Villingier, H., 1990. Analysis of conductive and convective heat transfer in a sedimentary basin, demonstrated for the Rheingraben. *Geophys. J. Int.* 100 (3), 393–414.
- Curtis, C.D., Murchison, D.G., Berner, R.A., Shaw, H., Santhein, M., Durand, B., Eglinton, G., Mackenzie, A.S., Surdam, R.C., 1985. Clay mineral precipitation and transformation during burial diagenesis (and discussion). *Phil. Trans. Roy. Soc. Lond. Math. Phys. Sci.* 315 (1531), 91–105.
- Dachroth, W., 1985. Fluvial sedimentary styles and associated depositional environments in the Buntsandstein west of river Rhine in Saar area and Pfalz (F.R. Germany) and Vosges (France). In: Mader, D. (Ed.), *Aspects of Fluvial Sedimentation in the Lower Triassic Buntsandstein of Europe*. Springer-Verlag, Heidelberg, pp. 197–248.
- Deutsche Stratigraphische Kommission, 2016. In: Menning, M., Hendrich, A. (Eds.), *Stratigraphische Tabelle von Deutschland 2016*.
- Dezayes, C., Genter, A., Thinon, I., Courrioux, G., Tourlière, B., 2008. Geothermal potential assessment of clastic reservoirs (Upper Rhine Graben, France). *Thirty-Second Workshop on Geothermal Reservoir Engineering*. Stanford University, Stanford, California, pp. 1–8.
- Dezayes, C., Villemain, T., Genter, A., Traineau, H., Angelier, J., 1995. Analysis of fractures in boreholes of the hot dry rock project at Soultz-sous-Forêts (Rhine Graben, France). *Sci. Drill.* 5, 31–41.
- Dubois, M., Ayt Ougoudal, M., Meere, P., Royer, J.-J., Boiron, M.-C., Cathelineau, M., 1996. Temperature of paleo- to modern self-sealing within a continental rift basin: the fluid inclusion data (Soultz-sous-Forêts, Rhine graben, France). *Eur. J. Mineral.* 8, 1065–1080.
- Düringer, P., Aichholzer, C., Orciani, S., Genter, A., 2019. The complete lithostratigraphic section of the geothermal wells in Rittershoffen (Upper Rhine Graben, eastern France): a key for future geothermal wells. *BSGF - Earth Sciences Bulletin* 190. <https://doi.org/10.1051/bsgf/2019012>.
- Esch, W.L., Ajdukiewicz, J.M., Reynolds, A.C., 2008. Early grain-coat formation in Chaco Dune Field, New Mexico: insight into formation mechanisms, distribution, and implications for predictive modeling to assist in deep play identification. *AAPG Annual Convention*. AAPG, San Antonio, TX, p. 20.
- Feist-Burkhardt, S., Götz, A.E., Szulc, J., Borkhataria, R., Geluk, M., Haas, J., Hornung, J., Jordan, P., Kempf, O., Michalik, J., Nawrocki, J., Reinhardt, L., Ricken, W., Röhlhling, H.-G., Rüffer, T., Török, Á., Zühlke, R., 2008. Triassic. In: McCann, T. (Ed.), *The Geology of Central Europe Volume 2: Mesozoic and Cenozoic*. Geological Society of London, pp. 749–821. <https://doi.org/10.1144/cev2p.1>.
- Folk, R.L., 1980. *Petrology of Sedimentary Rocks*. Hemphill Publishing Company, Austin, Texas, U.S.A., p. 182.
- Folk, R.L., Ward, W., 1957. Brazos River bar: a study in the significance of grain-size parameters. *J. Sediment. Petrol.* 27, 3–26. <https://doi.org/10.1306/74D70646-2B21-11D7-8648000102C1865D>.
- Füchtbauer, H., 1974. Zur Diagenese fluviatiler Sandsteine. *Geol. Rundsch.* 63, 904–925.
- Gaupp, R., Okkerman, J.A., 2011. Diagenesis and reservoir quality of Rotliegend sandstones in the northern Netherlands - a review. In: Grötsch, J., Gaupp, R. (Eds.), *The Permian Rotliegend of the Netherlands*. Society for Sedimentary Geology, pp. 193–226.
- Greene, G.W., Kristiansen, K., Meyer, E.E., Boles, J.R., Israelachvili, J.N., 2009. Role of electrochemical reactions in pressure solution. *Geochem. Cosmochim. Acta* 73, 2862–2874. <https://doi.org/10.1016/j.gca.2009.02.012>.
- Griffiths, L., Heap, M.J., Wang, F., Daval, D., Gilg, H.A., Baud, P., Schmittbuhl, J., Genter, A., 2016. Geothermal implications for fracture-filling hydrothermal precipitation. *Geothermics* 64, 235–245. <https://doi.org/10.1016/j.geothermics.2016.06.006>.
- Haffen, S., Gérard, Y., Diraison, M., 2015. Geothermal, structural and petrophysical characteristics of Buntsandstein sandstone reservoir (Upper Rhine Graben, France). In: *World Geothermal Congress 2015*, pp. 1–12. Melbourne, Australia.
- Heald, M.T., 1955. Stylolites in sandstone. *J. Geol.* 63, 101–114. <https://doi.org/10.1086/626237>.
- Heald, M.T., Larese, R.E., 1974. Influence of coatings on quartz cementation. *J. Sediment. Petrol.* 44 (4), 1269–1274. <https://doi.org/10.1306/212F6C94-2B24-11D7-8648000102C1865D>.
- Heap, M.J., Kushnir, A.R.L., Gilg, H.A., Wadsworth, F.B., Reuschlé, T., Baud, P., 2017. Microstructural and petrophysical properties of the Permo-Triassic sandstones (Buntsandstein) from the Soultz-sous-Forêts geothermal site (France). *Geoth. Energy* 5, 1. <https://doi.org/10.1186/s40517-017-0085-9>.
- Held, U.C., Günther, M.A., 1993. *Geologie und Tektonik der Eisenerzlagerstätte Nothweiler am Westrand des Oberrheingrabens*. In: Rothe, P. (Ed.), *Jahresberichte und Mitteilungen des Oberrheinischen Geologischen Vereines*. Schweizerbart'sche Verlagsbuchhandlung (Nägele und Obermiller). Stuttgart, Germany, pp. 197–215.

- Horn, P., Lippolt, H.J., Todt, W., 1972. Kalium-Argon-Altersbestimmungen an tertiären Vulkaniten des Oberrheingraben-Gebietes: I. Gesamtgesteinsalter. *Eclogae Geologicae Helveticae* 65, 131–156.
- Houšeknecht, D.W., 1987. Assessing the relative importance of compaction processes and cementation to reduction of porosity in sandstones. *AAPG (Am. Assoc. Pet. Geol.) Bull.* 71, 633–642.
- Junghans, W.-D., 2003. Fazies, Zyklizität, Petrophysik und Paläomagnetik im Buntsandstein der Bohrung Kraichgau 1002 (SW-Deutschland), p. 191. Tübingen, Germany.
- Keller, J., Kraml, M., Henjes-Kunst, F., 2002. 40Ar/39Ar single crystal laser dating of early volcanism in the Upper Rhine Graben and tectonic implications. *Schweizerische mineralogische und petrographische Mitteilungen* 82, 121–130.
- Kristiansen, K., Valtiner, M., Greene, G.W., Boles, J.R., Israelachvili, J.N., 2011. Pressure solution - the importance of the electrochemical surface potential. *Geochem. Cosmochim. Acta* 75, 6882–6892. <https://doi.org/10.1016/j.gca.2011.09.019>.
- Kunkel, C., Aehnelt, M., Pudlo, D., Kukowski, N., Totsche, K.U., Gaupp, R., 2018. Subsurface aquifer heterogeneities of Lower Triassic clastic sediments in central Germany. *Mar. Petrol. Geol.* 97, 209–222. <https://doi.org/10.1016/j.marpetgeo.2018.06.022>.
- Lander, R.H., Larese, R.E., Bonnell, L.M., 2008. Toward more accurate quartz cement models: the importance of euhedral versus noneuhedral growth rates. *AAPG (Am. Assoc. Pet. Geol.) Bull.* 92 (11), 1537–1563. <https://doi.org/10.1306/07160808037>.
- Lander, R.H., Walderhaug, O., 1999. Predicting porosity through simulating sandstone compaction and quartz cementation. *AAPG (Am. Assoc. Pet. Geol.) Bull.* 83 (3), 433–449. <https://doi.org/10.1306/00AA9BC4-1730-11D7-8645000102C1865D>.
- Lander, R.H., Walderhaug, O., Bonnell, L.M., 1997. Application of sandstone diagenetic modeling to reservoir quality prediction and basin history assessment, *Memorias del I Congreso Latinoamericano de Sedimentología*. Sociedad Venezolana de Geólogos, Caracas, Venezuela, pp. 373–386.
- Lanson, B., Beaufort, D., Berger, G., Bauer, A., Cassagnabère, A., Meunier, A., 2002. Authigenic kaolin and illitic minerals during burial diagenesis of sandstones: a review. *Clay Miner.* 37 (1), 1–22. <https://doi.org/10.1180/0009855023710014>.
- LGRB, 2023. GeORG Mapviewer. <https://maps.geopotenziale.eu/?app=georg&lang=en>. (Accessed 16 March 2023).
- Liewig, N., Clauer, N., 2000. K-Ar dating of varied microtextural illite in Permian gas reservoirs, northern Germany. *Clay Miner.* 35, 271–281. <https://doi.org/10.1180/000985500546648>.
- Lippmann, R., 2012. Diagenesis in Rotliegend, Triassic and Jurassic Clastic Hydrocarbon Reservoirs of the Central Graben, North Sea. Friedrich-Schiller-University, Jena, PhD, p. 283.
- Lundegard, P., 1992. Sandstone porosity loss-A "big picture" view of the importance of compaction. *J. Sediment. Petrol.* 62 (2), 250–260. <https://doi.org/10.1306/D42678D4-2B26-11D7-8648000102C1865D>.
- Makowitz, A., Lander, R.H., Milliken, K.L., 2006. Diagenetic modeling to assess the relative timing of quartz cementation and brittle grain processes during compaction. *AAPG (Am. Assoc. Pet. Geol.) Bull.* 90 (6), 873–885. <https://doi.org/10.1306/12190505044>.
- Molenaar, N., Felder, M., 2018. Clay cutans and the origin of illite rim cement: an example from the siliciclastic Rotliegend Sandstone in the Dutch Southern Permian Basin. *J. Sediment. Res.* 88 (5), 641–658. <https://doi.org/10.2110/jsr.2018.33>.
- Molenaar, N., Vaznyte, J., Bär, K., Šliaupa, S., 2021. Illite and chlorite cementation of siliciclastic sandstones influenced by clay grain cutans. *Mar. Petrol. Geol.* 132 <https://doi.org/10.1016/j.marpetgeo.2021.105234>.
- Monsees, A.C., Busch, B., Hilgers, C., 2021. Compaction control on diagenesis and reservoir quality development in red bed sandstones: a case study of Permian Rotliegend sandstones. *Int. J. Earth Sci.* 110 (5), 1683–1711. <https://doi.org/10.1007/s00531-021-02036-6>.
- Monsees, A.C., Busch, B., Schöner, N., Hilgers, C., 2020. Rock typing of diagenetically induced heterogeneities – a case study from a deeply-buried clastic Rotliegend reservoir of the Northern German Basin. *Mar. Petrol. Geol.* 113, 104163 <https://doi.org/10.1016/j.marpetgeo.2019.104163>.
- Neasham, J.W., 1977. The morphology of dispersed clay in sandstone reservoirs and its effect on sandstone shaliness, pore space and fluid flow properties. *SPE Annual Fall Technical Conference and Exhibition*. Denver, CO.
- Oelkers, E.H., Bjørkum, P., Murphy, W.M., 1996. A petrographic and computational investigation of quartz cementation and porosity reduction in North Sea sandstones. *Am. J. Sci.* 296 (4), 420–452.
- Paxton, S.T., Szabo, J.O., Ajdukiewicz, J.M., Klimentidis, R.E., 2002. Construction of an intergranular volume compaction curve for evaluating and predicting compaction and porosity loss in rigid-grain sandstone reservoirs. *AAPG (Am. Assoc. Pet. Geol.) Bull.* 86 (12), 2047–2067. <https://doi.org/10.1306/61EEDDFA-173E-11D7-8645000102C1865D>.
- Pfaff, K., Hildebrandt, L.H., Leach, D.L., Jacob, D.E., Markl, G., 2010. Formation of the Wiesloch Mississippi valley-type Zn-Pb-Ag deposit in the extensional setting of the Upper Rhine Graben, SW Germany. *Miner. Deposita* 45 (7), 647–666. <https://doi.org/10.1007/s00126-010-0296-5>.
- Pittman, E.D., Larese, R.E., Heald, M.T., 1992. Clay coats : occurrence and relevance to preservation of porosity in sandstones. In: Houseknecht, D.W., Pittman, E.D. (Eds.), *Origin, Diagenesis, and Petrophysics of Clay Minerals in Sandstones*. SEPM Special Publication, Tulsa, Oklahoma, U.S.A., pp. 241–256. <https://doi.org/10.2110/pec.92.47.0241>.
- Plain, E., 1993. Voraussetzungen und Grenzen der Bildung von Kohlenwasserstoff-Lagerstätten im Oberrheingraben. In: Rothe, P. (Ed.), *Jahresberichte und Mitteilungen des Oberrheinischen Geologischen Vereines*. Schweizerbart'sche Verlagsbuchhandlung (Nägele und Obermiller). Stuttgart, Germany, pp. 227–253.
- Prajapati, N., Gonzales, A.A., Selzer, M., Nestler, B., Busch, B., Hilgers, C., 2020. Quartz cementation in polycrystalline sandstone: insights from phase-field simulations. *JGR: Solid Earth*. <https://doi.org/10.1029/2019JB019137>.
- Prajapati, N., Selzer, M., Nestler, B., Busch, B., Hilgers, C., Ankit, K., 2018. Three-dimensional phase-field investigation of pore space cementation and permeability in quartz sandstone. *J. Geophys. Res. Solid Earth*. <https://doi.org/10.1029/2018jb015618>.
- Quandt, D., Busch, B., Schmidt, C., Hilgers, C., 2022. Diagenesis and controls on reservoir quality of Lower Triassic red bed sandstones (Buntsandstein) from a marginal basin facies, southwest Germany. *Mar. Petrol. Geol.* 142 <https://doi.org/10.1016/j.marpetgeo.2022.105744>.
- Reicherter, K., Froitzheim, N., Jarosiński, M., Badura, J., Franzke, H.-J., Hansen, M., Hübscher, C., Müller, R., Poprawa, P., Reinecker, J., Stackebrandt, W., Voigt, T., Eynatten, H.V., Zuchiewicz, W., 2008. Alpine tectonics north of the Alps. In: McCann, T. (Ed.), *The Geology of Central Europe Volume 2: Mesozoic and Cenozoic*. Geological Society of London, p. 53. <https://doi.org/10.1144/cev2p.7>.
- Reinhold, C., Schwarz, M., Bruss, D., Heesbeen, B., Perner, M., Suana, M., 2016. The Northern Upper Rhine Graben : re-dawn of a mature petroleum province? *Swiss. Bulletin for Applied Geology* 21 (2). <https://doi.org/10.5169/seals-658196>.
- Rimstidt, J.D., Barnes, H.L., 1980. The kinetics of silica-water reactions. *Geochem. Cosmochim. Acta* 62, 1851–1863. [https://doi.org/10.1016/0016-7037\(80\)90220-3](https://doi.org/10.1016/0016-7037(80)90220-3).
- Sanjuan, B., Millot, R., Innocent, C., Dezayes, C., Scheiber, J., Brach, M., 2016. Major geochemical characteristics of geothermal brines from the Upper Rhine Graben granitic basement with constraints on temperature and circulation. *Chem. Geol.* 428, 27–47. <https://doi.org/10.1016/j.chemgeo.2016.02.021>.
- Schmidt, C., Busch, B., Hilgers, C., 2020a. Compaction and cementation control on bleaching in Triassic fluvial red beds, S-Germany. *Z. Dtsch. Ges. Geowiss.* <https://doi.org/10.1127/zdgg/2020/0233>.
- Schmidt, C., Busch, B., Hilgers, C., 2020b. Lateral variations of detrital, authigenic and petrophysical properties in an outcrop analog of the fluvial Plattensandstein, Lower Triassic, Central Germany. *Z. Dtsch. Ges. Geowiss.* <https://doi.org/10.1127/zdgg/2020/0234>.
- Schöner, R., Gaupp, R., 2005. Contrasting red bed diagenesis: the southern and northern margin of the Central European Basin. *Int. J. Earth Sci.* 94 (5–6), 897–916. <https://doi.org/10.1007/s00531-005-0004-3>.
- Schumacher, M.E., 2002. Upper Rhine Graben: role of preexisting structures during rift evolution. *Tectonics* 21 (1), 6–17. <https://doi.org/10.1029/2001tc900022>, 6–1.
- Schwarzer, D., Littke, R., 2007. Petroleum generation and migration in the 'Tight Gas' area of the German Rotliegend natural gas play: a basin modeling study. *Petrol. Geosci.* 13, 37–62. <https://doi.org/10.1144/1354-079306-703>.
- Sheldon, H.A., Wheeler, J., Worden, R.H., Cheadle, M.J., 2003. An analysis of the roles of stress, temperature, and pH in chemical compaction of sandstones. *J. Sediment. Res.* 7, 64–71. <https://doi.org/10.1306/070802730064>.
- Sibley, D.F., Blatt, H., 1976. Intergranular pressure solution and cementation of the Tuscarora orthoquartzite. *J. Sediment. Petrol.* 46 (4), 881–896. <https://doi.org/10.1306/212F7081-2B24-11D7-8648000102C1865D>.
- Slunitschek, K., Kolb, J., Eiche, E., 2021. Lithium extraction from geothermal brines: modern adsorption method for raw material extraction. *Wiley Analytical Science Magazine*. Wiley.
- Soyk, D., 2015. Diagenesis and Reservoir Quality of the Lower and Middle Buntsandstein (Lower Triassic), SW Germany. Ruprecht-Karls-University, Heidelberg, p. 201. PhD thesis.
- Stephenson, L.P., Plumley, W.J., Placiauskas, V.V., 1992. A model for sandstone compaction by grain interpenetration. *J. Sediment. Res.* 62 (1), 11–22. <https://doi.org/10.1306/D4267875-2B26-11D7-8648000102C1865D>.
- Tamburelli, S., Di Giulio, A., Amadori, C., Consonni, A., Ortenzi, A., 2022. New constraint on burial and thermal history of Devonian reservoir sandstones in the Illizi-Ghadames basin (North Africa) through diagenetic numerical modelling. *Mar. Petrol. Geol.* 145 <https://doi.org/10.1016/j.marpetgeo.2022.105903>.
- van Houten, F.B., 1973. Origin of red beds: a review - 1961-1972. *Annu. Rev. Earth Planet Sci.* 1, 39–61. <https://doi.org/10.1146/annurev.ea.01.050173.000351>.
- Walderhaug, O., 1994a. Precipitation rates for quartz cement in sandstones determined by fluid-inclusion microthermometry and temperature-history modeling. *J. Sediment. Res.* A64, 324–333. <https://doi.org/10.2110/jsr.64.324>.
- Walderhaug, O., 1994b. Temperatures of quartz cementation in Jurassic sandstones from the Norwegian continental shelf - evidence from fluid inclusions. *J. Sediment. Res.* 64 (2), 311–323.
- Walderhaug, O., 1996. Kinetic modelling of quartz cementation and porosity loss in deeply buried sandstone reservoirs. *AAPG (Am. Assoc. Pet. Geol.) Bull.* 80, 731–745. <https://doi.org/10.1306/64ED88A4-1724-11D7-8645000102C1865D>.
- Walderhaug, O., Lander, R.H., Bjørkum, P.A., Oelkers, H., Bjørlykke, K., Nadeau, P.H., 2000. Modelling quartz cementation and porosity in reservoir sandstones: examples from the Norwegian continental shelf. In: Worden, R.H., Morad, S. (Eds.), *Quartz Cementation in Sandstones*. Blackwell Science Ltd., Oxford, pp. 39–49. <https://doi.org/10.1002/9781444304237.ch3>.
- Walker, T.R., 1979. Red color in dune sands. In: McKee, E.D. (Ed.), *A Study of Global Sand Seas*. U.S. Government Printing Office, Washington, D. C., pp. 61–81.
- Wendler, J., Köster, J., Götz, J., Kasch, N., Zisser, N., Kley, J., Pudlo, D., Nover, G., Gaupp, R., 2011. Carbonate diagenesis and feldspar alteration in fracture-related bleaching zones (Buntsandstein, central Germany): possible link to CO₂-influenced fluid-mineral reactions. *Int. J. Earth Sci.* 101 (1), 159–176. <https://doi.org/10.1007/s00531-011-0671-1>.
- Werner, W., 2012. Schätze unter dem Boden: Was wissen wir über die tiefliegenden Rohstoffe in Baden-Württemberg?. *Berichte der Naturforschenden Gesellschaft zu Freiburg im Breisgau*, vol. 102, pp. 37–92.

- Werner, W., Dennert, V., 2004. Lagerstätten und Bergbau im Schwarzwald. Landesamt für Geologie, Rohstoffe und Bergbau Baden-Württemberg 334. Freiburg, Germany.
- Wooldridge, L.J., Worden, R.H., Griffiths, J., Utley, J.E.P., 2017. Clay-coated sand grains in petroleum reservoirs: understanding their distribution via a modern analogue. *J. Sediment. Res.* 87 (4), 338–352. <https://doi.org/10.2110/jsr.2017.20>.
- Worden, R.H., Morad, S., 2000. Quartz Cementation in Oil Field Sandstones: A Review of the Key Controversies. In: Worden, R.H., Morad, S. (Eds.), *Quartz Cementation in Sandstones*. Blackwell Publishing Ltd., Oxford, pp. 1–20. <https://doi.org/10.1002/9781444304237.ch1>.
- Ziegler, P.A., 1990. In: *Geological atlas of western and central Europe* Shell Internationale Petroleum Maatschapij B.V., The Hague, p. 239.
- Ziegler, P.A., 1992. European Cenozoic rift system. *Tectonophysics* 208 (1–3), 91–111.